Supplemental Information for:

Mild depolarization of the inner mitochondrial membrane is a crucial component of an anti-aging program.

Mikhail Yu. Vyssokikh et al.

S1. History of the discovery of mild depolarization as a component of the anti-aging program

The concept of mild depolarization described above originates from three discoveries made in the second half of the XX century (Fig. S1). (a) In 1954, S. Bessman suggested (1) that hexokinase binds to mitochondria in such a way that ATP released from mitochondria directly approaches the catalytic site of the enzyme without dilution of the nucleotide in the cytosol ("hexokinase acceptor effect"). This hypothesis was subsequently confirmed by Bessman and colleagues as well as other researchers (2-7). (b) In 1961, P. Mitchel proposed his "chemiosmotic hypothesis", assuming that the difference in the transmembrane electric potentials in mitochondria is the main driving force for oxidative phosphorylation (8). In 1969, the idea of "mitochondrial electricity" was directly confirmed when our group together with the E. Liberman's group showed that synthetic penetrating ions are distributed in respiring mitochondria according to the Nernst equation, with cations and anions moving in opposite directions (9). (c) In 1971, B. Chance and coworkers reported (10, 11) that ADP phosphorylation in respiring mitochondria is accompanied by a complete inhibition of mROS formation. In 1997, S. Korshunov, V. Skulachev and A. Starkov reported (12) that the mild depolarization of the mitochondrial membrane by (i) a small decrease in the respiration rate, (ii) a small increase in the membrane H^+ conductance induced by protonophorous uncouplers or (iii) ADP addition inhibited the mROS-generating mechanism in Complex I.

In 2004-2008, A. Galina et al. (13-15) summarized findings reported in a, b and c branches and showed that rat brain mitochondria are equipped with a potent antioxidant system composed of mitochondria-bound hexokinase and creatine kinase. Rat liver mitochondria lack this antioxidant system. The antioxidant systems in the kidney and heart mitochondria appear to be much less effective than the system in the brain.

As shown in the present study, the brain is not the only organ that *completely* prevents mROS generation by mild depolarization of mitochondria. This phenomenon was also observed in the lung, kidney, heart, skeletal muscles, diaphragm and spleen but not in the liver (the latter observation was in line with the observations reported by Galina and colleagues (13-15)). Moreover, in aging mice, mild depolarization is decreased to some extent in the lung, brain and kidney and is completely blocked in the heart, skeletal muscles, diaphragm and spleen. The age-related inhibition of this antioxidant system results in oxidative stress, which is particularly severe

in the lower four tissues. In long-lived NMRs, no decrease in mild depolarization is observed during aging for up to at least 11 years. A similar effect was observed in a long-lived bat. It is suggested that mild polarization of mitochondria and its switching off represent an example of anti-aging and aging programs, respectively.

S2. General schemes illustrating the mechanisms of mild depolarization

Apparently, a high $\Delta\psi$ is required for the one-electron reduction of O_2 to superoxide by a Complex I-associated redox center (probably by the FeS1a cluster, which is the only Complex I redox center requiring mitochondrial hyperpolarization for its reduction). The addition of a small amount of ADP with glucose or creatine decreases $\Delta\psi$ from 190 to 150 mV (mild depolarization), which entails the oxidation of the abovementioned redox center and subsequently *completely* inhibits $O_2^{\bullet-}$ formation.

Figs. 1 and S2 illustrate the interrelationships of respiratory chain electron transport (Complexes I, II, III and IV), H^+-ATP-synthase (Complex V, also known as F_0F_1), the ATP and ADP transporters (ATP/ADP antiporter and porin) and hexokinase I or II bound to porin. The steps in $\Delta\psi$ generation and utilization, as well as mROS formation, are also shown. Succinate is presumed to represent one of the major sources of electrons for mROS generation in Figs. 1 and S2. Based on accumulating evidence, succinate is oxidized by the respiratory chain to generate the highest $\Delta\psi$, which supports reverse electron transfer via Complex I to NAD^+ and the reduction of O_2 to superoxide. Several metabolic pathways have already been identified as sources for succinate, namely, the Krebs cycle, glutamine (16, 17), and propionyl CoA (18), and as sources for fumarate, aspartate or adenylsuccinate (19). Usually, a substantial increase in the succinate concentration accompanies oxidative stress initiated by some regulatory systems of the cells (16, 17, 19-21). Apparently, succinate plays a crucial role in generating mROS because it functions as a respiratory substrate to support the maintenance of the highest $\Delta\psi$ compared with all the other respiratory substrates. This result is partially due to the high concentrations of Complex II (succinate dehydrogenase) and its immersion in the hydrophobic core of the inner mitochondrial membrane, in contrast to other Krebs cycle dehydrogenases that are located on the membrane surface or in the mitochondrial matrix. CoQ, the electron acceptor of Complex II, is very hydrophobic. It transports electrons to Complex III or I. The carriers participating in electron transport from $CoQH_2$ to O_2 to form H_2O and $\Delta\psi$ do not require the participation of Complex I, which is, however, obligatory if NAD-linked substrates are used. Complex I catalyzes the slowest step of the respiratory chain. Therefore, the pathway involving Complexes II, III and IV potentially generates a larger $\Delta\psi$ than the pathway involving Complexes I, II and IV (21).

Unfortunately, the mechanism responsible for mROS generation under reverse electron transfer via Complex I remains obscure. The hyperpolarization of the inner mitochondrial membrane is required for reverse electron transfer and mROS formation, but the molecular aspects of these two phenomena are not yet known.

S3. Mild depolarization is inherent in hexokinase-linked glycolysis but not in ketohexokinase-linked fructolysis

The disappearance of mild depolarization in the mouse liver after birth does not occur in NMRs at least up to 11 years of age. As reported by Th. J. Park et al. (22, 23), NMRs mainly utilize fructose instead of glucose as a carbohydrate monomer. The source of fructose is currently unknown. Both the fructose transporter in the outer cell membrane of this organism and the enzyme initiating fructolysis (ketohexokinase, KHK) are expressed at higher levels than the glucose transporter and hexokinases (HK) (Fig. S24). As shown in the same figure, mild depolarizing mechanisms requiring hexokinases are indicated by reactions 12 and 14. When G6P, the product of glucose phosphorylation, accumulates in the cytosol, it stimulates the dissociation of hexokinases from mitochondrial porin and subsequently inhibits mild depolarization. This inhibition does not occur during fructolysis since its products (F6P and F1P) fail to dissociate the hexokinase-porin complex (24, 25). Moreover, ketohexokinase-mediated fructolysis bypasses the crucial step of downregulating aerobic glycolysis at the level of phosphofructokinase (PFK), an enzyme that is involved in carbohydrate decomposition initiated by hexokinases but not by ketohexokinase. PFK is allosterically inhibited by one of its substrates (ATP), which is produced by the final reactions of respiration and glycolysis. Citrate, the first tricarboxylic acid in the Krebs cycle, is also a PFK inhibitor. Moreover, PFK is very sensitive to the acidification of the medium, which inevitably occurs during the terminal step of glycolysis, i.e., the dissociation of lactic acid to lactate anion and H^+. None of these PFK inhibitors block the main fructolytic pathway mediated by F1P. Resistance to acidification is particularly important since an acidic pH shift, which occurs when glucose is converted to lactate, can result in the protonation of superoxide: $O_2^{\bullet-} + H^+ \rightarrow HO_2^{\bullet}$. The product ($HO_2^{\bullet}$) is a poison as dangerous as $OH^{\bullet}$. Superoxide is generated by the mitochondrial respiratory chain. $O_2^{\bullet-}$ is of rather low toxicity *per se*, but it can be converted to very toxic products as a result of (a) its protonation, (b) its reaction with NO or (c) conversion to the $OH^{\bullet}$ radical via H_2O_2, which is catalyzed by Fe^{2+} or Cu^+:

$O_2^{\bullet-} \rightarrow H_2O_2 \xrightarrow{Fe^{2+},\ Cu^+} OH^{\bullet}$ (c).

The protonation of $O_2^{\bullet-}$ does not require H_2O_2, Fe^{2+} or Cu^+.

The tissue damage induced by anaerobic glycolysis does not occur during *anoxia* ($O_2^{\bullet-}$ is not formed since O_2 is absent) but is observed during *reoxygenation* when O_2 appears; $O_2^{\bullet-}$ is formed by the mitochondria, and the H^+ ion (formed during the preceding anoxia) protonates superoxide. We suggest that mitochondrial $O_2^{\bullet-}$ generation increases due to the activation of the aging program, but in NMRs, this program is substantially inhibited. Therefore, NMRs use fructolysis, which is not limited by H^+-mediated control of PFK.

Thus, fructose catabolism via the hexokinase pathway (Fig. S24, reaction 11) effectively participates in the mild depolarization of the mitochondria as a crucial component of their antioxidant system. In contrast to fructolysis, G6P-forming glucose catabolism contributes to the development of pathologies such as diabetes associated with high ROS levels due to the inhibition of mild depolarization by G6P (13, 26). Hyperglycemia occurs in response to the dysfunctional insulin regulation of glucose metabolism and induces G6P superproduction and the subsequent desorption of hexokinases from porin, an event that inhibits the mild depolarization system. As shown by Galina and colleagues (13, 26), the accumulation of excess G6P and mitochondrial hyperpolarization induce the apoptosis of brain cells.

S4. Alternative aging programs

The disappearance of mild depolarization with aging is probably a result of the activation of *an aging program* that inhibits anti-aging programs (27, 28). The existence of an aging program was postulated by August Weismann at the end of the XIX century (29). This hypothesis was revisited at the end of the XX century following the discovery of apoptosis, a type of programmed cell death occurring in multicellular organisms (30). Recently, it was found that bacteria and unicellular eukaryotes are also equipped with special suicide mechanisms, which in yeast were mechanistically similar to apoptosis (31).

The self-elimination of a living organism was designated “phenoptosis” (32-34). Biological aging represents a case of slow (chronic) phenoptosis (32-35). In 2017-2018, two groups independently showed that the aging of a multicellular organism (*C. elegans*) is a programmed process required to stimulate the production of eggs by obtaining additional substrates for egg biosynthesis (36-39).

It was postulated that programmed aging is beneficial for evolution due to the acceleration of changes in successive generations (29, 32). Within the framework of this concept, aging is a facultative process regulated by an organism that is equipped with competing aging and anti-aging programs (27, 40). In 2016 and 2017, our group postulated that the exclusive longevity of NMRs is a consequence of neoteny, i.e., prolongation of youth by the strong retardation of ontogenesis; we concluded that aging is an ontogenetic subprogram (28, 40, 41).

A question arises as to why the aging program, which is clearly counterproductive for the individual, was not eliminated by biological evolution. In fact, this type of program is well known, but its appearance during evolution is still a mystery. Sexual reproduction is one of the best examples of this problem. This process is counterproductive for parents but very productive for the evolution of their children and the species. Similarly, Schmalhausen's *conservative evolution theory* states that sexual reproduction is responsible for the existence of the present genotype (42, 43). Conservative evolution tries to eliminate any new traits, in contrast to Darwin's dynamic evolution based on the appearance of these traits.

One possible way to solve the problem for aging programs is to activate *several parallel pathways* resulting in aging. A mutation in a component of one pathway would not be sufficient for elimination of aging. Nrf2 is an example of such a situation. This protein operates as a key component of the anti-aging program represented by antioxidant enzymes (the third line of anti-ROS defense, Table S1). Nrf2 induces the expression of several genes encoding antioxidant enzymes. As mentioned above, the levels of these enzymes are decreased with aging in the majority of mouse tissues (Table S2). This effect might be related to the decrease in the level of Nrf2 in old mice (44-47). The Nrf2 decrease can be mediated by at least four different proteins that inhibit Nrf2, namely, KEAP1, Bach 1, β-TrCP and c-Myc (48-50). All of these proteins might be considered as components of an aging program. The first three proteins are inhibited by ROS, which makes the situation even more complicated than the simple competition of anti-aging and aging programs.

An additional pathway preventing the elimination of the aging program is based on the observation that Complex I is *the main*, but not *the only*, source of mROS that mediate aging. (i) Under certain patological conditions, Complex III produces up to 20% of mROS (51). (ii) Cytochrome *c*, which normally functions as an electron carrier from Complex III to Complex IV, can interact with another protein, p66shc. The cytochrome c • p66shc complex reduces O_2 to $O_2^{\bullet -}$ without requiring any other enzymes. Knockout of the p66shc gene increases the lifespan of animals by 30% (52-54). (iii) Monoaminoxidase is located on the outer surface of the outer mitochondrial membrane. Its activity increases by 7.5-fold with aging (55). This oxidase converts O_2 to H_2O_2. The contribution of this enzyme to mROS generation is limited by the low concentrations of monoamines in the cell. (iv) Dihydrolipoate dehydrogenase, a component of multienzyme complexes that decarboxylate pyruvate and α-ketoglutarate, produces H_2O_2 in the mitochondrial matrix. The process is strongly activated by NH_3 (56).

S5. Mild depolarization: from mammals to plants

Originally, Galina and coworkers (13-15) postulated that maximal kinase-mediated ADP cycling occurs in the brain, lower levels are observed in the kidney and the process does not occur in the liver. We confirmed the hypothesis by showing that in adult mice, the highest mitochondria-bound hexokinase level is observed in the brain and the lowest level is observed in the liver, with the kidney occupying an intermediate position. However, not only the brain but also the heart, kidney, skeletal muscle, diaphragm, lung and spleen contained sufficient amounts of mitochondria-bound hexokinases to *completely* inhibit mROS generation at a physiological glucose level. Why did Brazilian biochemists fail to observe this phenomenon that is inherent in the majority of mammalian tissues? First, they did not study the skeletal muscle, diaphragm, lung and spleen, i.e., tissues exhibiting mild depolarization observed in the present study. Second, in the skeletal muscles, the mitochondrial hexokinase isozyme belongs to class II (rather than isozyme I in other tissues), which has a low affinity for glucose. If researchers attempt to identify the mild depolarization of muscle mitochondria, then much higher concentrations of glucose are required than those in brain mitochondria. Third, the mild depolarization phenomenon disappears during the incubation of mitochondria with glucose *in vitro*, partially due to the accumulation of G6P, an inhibitor of hexokinase and a substance that desorbs hexokinase from mitochondria. Nevertheless, in our experiments, mild depolarization was a highly reproducible event observed in eight studied mouse tissues, except for the liver. Notably, several independent publications seem to indicate that some other mammalian tissues, in addition to the brain, contain mitochondria-bound hexokinases (57-59).

Recently, Galina and colleagues (60) described a bound hexokinase mechanism in plant mitochondria isolated from potato tubers. The mitochondria-bound hexokinase has a higher affinity for glucose than fructose (K_m values of 140 μM and 1.375 mM, respectively). Glucose stimulated State 4 succinate oxidation by factor 8 and inhibited H_2O_2 formation. To obtain the same inhibition by soluble yeast hexokinase, a 100-fold higher amount of the enzyme was needed than in the case of mitochondria-bound hexokinase.

S6. Diabetes and Alzheimer's disease

Apparently, mild depolarization mechanisms are widespread among mitochondria-containing organisms. This predicts the existence of pathologies related to some type of damage to such a sophisticated antioxidant system. Diabetes might be caused by hyperproduction of G6P inducing desorption of hexokinases from the mitochondria (13, 15).

A drug that functions as a mild depolarizer could be developed. Synthetic penetrating cations might be candidate drugs. As reported by Saraiva et al. (61), the brain accumulation of amyloid β-peptide (Aβ) during Alzheimer's disease causes the dissociation of hexokinase I from the mitochondria and increases mROS levels. These effects are prevented by adding 2DOG to

neurons. Unfortunately, 2DOG has a side effect: it blocks the formation of G6P by hexokinase. The blockade inhibits glucose catabolism. Our group showed that the penetrating cations SkQ1 and C_{12}TPP replaced 2DOG without inducing any undesirable side effects.

S7. The brain triad described by Antonio Galina: mitochondria, hexokinase and calcium

When we had completed this study, A. Galina and coworkers published an article (51) detailing a role for bound hexokinase in the clearance of cytosolic Ca^{2+}. The mechanism consists of the electrophoretic translocation of Ca^{2+} from the cytosol to the mitochondrial matrix. The production of mROS by Complex I damages the inner mitochondrial membrane, which becomes leaky for H^+ ions, competing with Ca^{2+} ions for $\Delta\psi$. 2DOG prevented this damage and hence stimulated Ca^{2+} uptake by energized mitochondria. The authors stressed that this mechanism may control intracellular ion homeostasis in the brain. Other tissues also requiring Ca^{2+} homeostasis were not studied.

S8. Concluding remarks

We confirmed the observations reported by A. Galina and coworkers (13-15) that murine brain mitochondria bind hexokinase and creatine kinase to utilize mitochondria-produced ATP. ADP, which is generated from ATP in bound kinase catalytic sites, is transported back to the mitochondrial matrix without dilution in the cytosol. As a result, the rate of ADP formation is stabilized at a high level required for the fast utilization of $\Delta\psi$ by H^+-ATP-synthase. This event subsequently decreases the $\Delta\psi$ below the level required to generate mROS.

We found that this process is not specific to the brain. In seven of eight studied adult mouse tissues, mitochondria-bound hexokinases I and II and creatine kinase are observed, and their activities are sufficient to completely prevent mROS generation [for a description of the physiological concentrations of glucose and creatine, see refs. (62, 63)]. The only exclusion is the liver because this organ utilizes lactate produced by the muscles during intensive physical work (the Cori cycle). In mouse embryos and in adults of very long-lived NMRs, the liver is also equipped with this antioxidant mechanism which we designated mitochondrial *mild depolarization*.

In mouse skeletal muscles, diaphragm, heart, brain and spleen, the maximal levels of bound hexokinases are observed in 3-month-old animals [see also (51)]. The levels decrease in 12-, 24- and 30-month-old animals, and thus, sugar- and creatine-mediated mild depolarization disappears. In the liver, mild depolarization disappears immediately after birth. In the lung and kidney, it partially decreases during aging but is compensated to some extent by catalase and other less-

effective antioxidant mechanisms that degrade the already formed ROS rather than prevent their formation. The mechanisms in question are mediated by catalase, glutathione peroxidase and glutathione reductase (Table S2). As a result, the malondialdehyde and protein carbonylation levels are substantially increased with aging in the mouse muscles, diaphragm, heart, brain and spleen and to a lesser (but still significant) extent in lung and kidney. Mild depolarization has been proposed as a mechanism of the *anti-aging program.* Age-induced suppression of mild depolarization should be regarded as a component of the *aging program* initiating mROS generation. In the mouse, this aging program begins at the age of one year. In the NMR, the aforementioned suppression does not occur at ages up to 11 years, resulting in the longevity of NMRs, which are resistant to the effects of mROS as aging mediators (28, 64-66).

The short-lived mouse and long-lived NMR form a nice pair of mammals to study the competition between the aging and anti-aging programs. A comparison of these two species prompted our hypothesis that other animals with a long lifespan should, in contrast to mice, maintain mild depolarization for a long period of life. To verify this hypothesis, we measured the effect of glucose on State 4 respiration in the mitochondria of a bat with a lifespan of up to 17 years. This old animal still possessed very strong stimulation of State 4 respiration by glucose.

Apparently, the aging program, similar to other ontogenetic programs, should be controlled by the Master biological clock (67, 68), which, unfortunately, has not yet been identified. It is probably located in the suprachiasmatic nucleus of the hypothalamus, which is responsible for circadian and seasonal rhythms. Apparently, the clock sends signals to inhibit the mild depolarization machinery, which in young animals prevents the mROS-mediated poisoning of the organism. The inhibition of mild depolarization in older animals occurs due to (a) a decrease in the expression of the hexokinase I and II and creatine kinase genes [this paper and ref. (69)] and (b) the binding of an inhibitory protein, PUM2, to hexokinase II mRNA (70-72). Subsequently, hexokinase and creatine kinase levels in the cytosol are decreased below the threshold required for their binding to mitochondria and mild depolarization. Moreover, the desorption of hexokinases from mitochondria can be induced by the special TAT peptide. Its level increases with age (57, 73). An additional mechanism for inhibiting depolarization may be related to the accumulation of G6P in the cells. This product of the hexokinase reaction (i) desorbs hexokinases from the mitochondria and (ii) inhibits their enzyme activity. Moreover, aging is accompanied by a decrease in the levels of antioxidant enzymes and GSH. Among the enzymes, catalase, GPx and GR are particularly important. Remarkably, in mice, hepatocytes express catalase at very high levels, which do not decrease with aging. In other tissues, the age-linked decrease in the activity of antioxidant enzymes is apparently mediated by a decrease in the level of Nrf2, a protein that induces the expression of genes encoding these enzymes (see above, Section S4)

We identified an additional delicate pro-aging mechanism in skeletal muscles. In mouse embryos, mild depolarization occurs at rather low levels since mROS production is limited by low [O_2]. In 3-month-old mice, depolarization increases, mainly due to an increase in hexokinase II levels (low affinity for glucose) rather than hexokinase I (high affinity for glucose). In 2.5-year-old mice, mild depolarization in muscles is completely lost due to the inhibition of the expression of both hexokinases I and II.

In long-lived NMRs, hexokinase II is expressed at high levels in muscles only at 3 years of age. In the muscles of 3-month-old NMRs, the contents of the two hexokinases are equal. A decrease in total hexokinase-linked depolarization does not occur in NMRs with aging. Catalase levels exhibit a slight decrease. The anti-aging activities of two protein kinases, i.e., the serine/threonine kinase DMPK and tyrosine kinase Src, should receive special attention. They stimulate hexokinase II binding to the mitochondria (74). The protein kinase Akt facilitates the interaction of hexokinase II with porin (75-78).

These and some other as yet unknown components of the anti-aging and aging programs will be attractive targets of future gerontological investigations designed to stop aging and prolong youth.

S9. Materials and methods

Animal housing and care. F1 hybrids of C57Bl/6/CBA mice were obtained by crossing parent mice from the SPF animal house of the Institute of Cytology and Genetics, Novosibirsk, Russia.

NMR colonies were housed in independent habitat systems consisting of 4-8 Plexiglas cylinders with a diameter of 25 cm and a size of 22/30 cm; the cylinders were connected by a system of Plexiglas pipes (a diameter, 5 cm). Habitats were maintained at a temperature of 27 ± 1.5°C, and the humidity ranged from 30% to 60%. The diet did not include drinking water but included a variety of fruits, vegetables and cereals and special feed for small laboratory rodents. Some cardboard cylinders were placed in the labyrinths.

Each NMR was implanted with a chip containing information about the date of birth. The sex of every animal was determined by analyzing the DNA obtained from a skin sample collected during chip insertion at the age of 1 month using RT-PCR (see below).

Tissue sampling. Tissue samples were obtained from mouse embryos (18 days) and 3-, 12- and 30-month-old F1 C57Bl/6/CBA hybrid mice. Prior to sampling, all animals were euthanized by cervical dislocation, according to the recommendations of the Ethics Committee. The head was removed, and forebrains were collected. The other tissues were collected in the following order, and the sizes of the samples are listed: heart, lung (left), diaphragm, spleen, kidney - whole organ,

liver - half of the organ, and whole leg muscle (*femoralis major*). After sampling, tissue fragments or whole organs were cut into 3 pieces. One small fragment was stored in RNALater solution (Thermo Fisher Scientific, USA), and another was stored in RIPA buffer in liquid nitrogen for further isolation of RNA and PAAG/WB analysis. The largest fragment was used for the subsequent isolation of mitochondria. Samples of 20- to 30-year-old NMRs kept in liquid nitrogen were used.

Isolation of mitochondria from mouse and NMR tissues. In all cases, tissue fragments were cut into 0.5-1-mm pieces and homogenized with Potter Teflon–glass microhomogenizer with 200 micron clearance in 10 volumes (v/w) of 300 mM mannitol, 0.5 mM EGTA, 20 mM HEPES-NaOH, pH 7.6, and 0.1% BSA (isolation medium) for 2 min at 4°C, with a ratio of 10/1 volume to weight of tissue fragment. The homogenate was centrifuged at 1000 *g* for 10 min at 4°C in an Eppendorf centrifuge (Germany). The supernatant was collected and centrifuged at 9000 *g* under the same conditions. Mitochondrial pellets were collected and suspended in the same volume of isolation medium lacking BSA (a microhomogenizer and centrifugation at 10,500 *g* for 10 min at 4°C were used). The resulting pellet was suspended in a minimal volume with a typical concentration of 90-100 mg/ml, as determined using the bicinchoninic acid method with BSA as the standard, according to the manufacturer's instructions (Pierce, USA).

Mitochondria were also isolated from the tissues of 18-day-old mouse embryos using the method described by Nyquist-Battie and Freter (79). Cesarean sections were performed on gestational day 18 after anesthesia induced by ether inhalation. All mouse pups were weighed and then euthanized by cervical dislocation. The heart, liver, brain, lung, kidney, spleen, diaphragm or leg muscles were dissected and used to isolate mitochondria with the procedure described above for tissues from adult animals.

Mitochondrial respiration measurement. The respiratory activity of isolated mitochondria was measured polarographically with a Clark-type electrode on a Hansatech instrument (Hansatech, UK) in an all-glass reaction chamber with magnetic stirring at 25°C. The mitochondrial pellet was suspended to obtain a final concentration of 0.1 mg/ml in the medium containing 220 mM mannitol, 10 mM potassium lactobionate, 5 mM KH_2PO_4, 2 mM $MgCl_2$, 10 μM EGTA, and 20 mM HEPES-KOH, pH 7.6 (MIR05, Oroboros, Austria). State 2 respiration was initiated by adding succinate (10 mM). The maximal respiration rate was induced by the addition of either 100 μM ADP (State 3) or 10 nM FCCP (State 3u). Potassium cyanide (0.5 mM) was added in the last step.

Western blot analysis. Samples were reduced to a powder in liquid nitrogen, lysed with ice-cold RIPA buffer, sonicated with 3 pulses of 10 s each using a VibraCells Ultrasonic Processor (Sonics, USA), and incubated at 65°C for 5 min. Afterwards, an equal volume of loading buffer was added. Samples were stored at -20°C until use and heated at 65°C for 5 min before loading. Proteins were separated using 10% sodium dodecyl sulfate polyacrylamide gel electrophoresis (SDS-PAGE) and transferred to a nitrocellulose membrane (Millipore, USA) under wet conditions using CAPS buffer (10 mM CAPS and 10% ethanol, pH 11). Membranes were blocked with 5% milk in Tris-buffered saline containing 0.1% Tween (TTBS) for 1 h at room temperature. Blots were incubated with primary (anti-HK1, ab65069, 1:1000; anti-HK2, ab37593, 1:2000; anti-Tubulin, ab18251, 1:10,000; and anti-VDAC1, ab154856, 1:2000; Abcam, USA) and peroxidase-conjugated secondary antibodies in 5% milk/TTBS for 1 h at RT. Target proteins were visualized using a Novex ECL Kit (Invitrogen, USA) and a ChemiDoc station (Bio-Rad, USA). The optical density of the protein bands was measured using ChemiDoc software, and band densities were normalized to tubulin as a marker of the cytosolic fraction and porin as a marker of the mitochondrial fraction. Representative blots from different mouse tissues are shown in Fig. S25.

Determination of the mitochondrial membrane potential (Δψ). The mitochondrial Δψ measurement was performed in a mitochondrial suspension by monitoring the changes in the fluorescence of safranin O (final concentration, 4.3 μM) at excitation/emission wavelengths of 485/586 nm using a Cary Eclipse fluorescence spectrophotometer (Agilent Technologies, USA). A mitochondrial suspension containing 0.05 mg protein was placed in a cuvette containing 1 ml of MIR05 (see above) with 10 mM succinate and 2 mM rotenone and incubated at 25°C. The gradual dissipation of the mitochondrial Δψ was assessed with stepwise additions of 10^{-8} M FCCP up to 30 nM. Data were calibrated using a K^+ gradient, as described by Figueira and colleagues (80). A calibration curve was fitted using Prism software (GraphPad, USA).

Hydrogen peroxide production. The hydrogen peroxide produced by mitochondria was analyzed as described in a previous study (81) using Amplex Red reagent (10-acetyl-3,7-dihydroxyphenoxazine; Invitrogen, USA) and horseradish peroxidase (Thermo Fisher Scientific, USA) on a Cary Eclipse fluorescence spectrophotometer (Agilent Technologies, USA), with the modifications described in our previous study (82).

RNA isolation. Tissue samples were homogenized in liquid nitrogen by grinding in a ceramic mortar. The powder was dissolved in 1 ml of Extract RNA Reagent (Evrogen, Russia). All procedures were performed according to the manufacturer's protocol. RNA concentrations and 260/280 ratios were measured with a DS-11 spectrophotometer (DeNovix, USA). For the reverse transcription reaction, 0.5 μg total RNA was reverse transcribed using MMLV-RT kits (Evrogen, Russia).

Real-time quantitative RT-PCR. The expression of specific mRNAs was quantified using a DT-96 thermocycler (DNA-Technology LLC, Russia). Real-time PCRs were conducted in triplicate in a reaction volume of 10 µl containing 100 ng cDNA, 300 nM each primer and 2 µl 5x SYBR Green mix (Evrogen, Russia). All primer sequences were generated and verified for specificity by Primer-BLAST. Next, 1.5% agarose gel electrophoresis and a melting curve analysis were used to estimate the amplicon size and primer specificity. The PCR program consisted of an initial step at 95°C for 5 min; 45 cycles of denaturation at 95°C for 10 s, annealing at 60°C for 20 s and elongation at 67°C for 20 s; and then melting at a gradient from 65°C to 95°C. Relative gene expression was determined as the ratio of the expression of the target gene to the expression of the internal reference gene (β-actin) based on Ct values using QGENE software.

HK enzyme activity assay. The method employed to analyze HK activity was based on the protocol reported by Scheer et al. (83). The assay buffer contained 50 mM Tris-HCl, 5 mM mercaptoethanol, 5 mM ATP, 10 mM MgCl2, 0.5 mM glucose, 0.8 mM NAD^+ and 1 U/ml G6P dehydrogenase from *Leuconostoc mesenteroides* (Roche) at pH 7.5. All assays were performed at 25°C in a total volume of 1.0 ml, and activity was determined using a Cary Varion 300 spectrophotometer. Enzyme activity was monitored by measuring the increase in absorbance at 340 nm, where 1 unit of enzyme was defined as the amount that catalyzed the conversion of 1 µmol of substrate to products within 1 min. HK activities were reported as the soluble, bound or total activities per total milligram of protein. The assay data are reported as the means ± S.E.M. from three or more experiments.

Catalase, SOD and GPx1 activity assays. The enzymatic activities of catalase, superoxide dismutase and glutathione peroxidase I in tissue extracts were measured using a Catalase Activity Assay Kit (Abcam, ab83464), Superoxide Dismutase Activity Assay Kit (Abcam, ab65354) and Glutathione Peroxidase Activity Kit (Abcam, ab102530), respectively, according to the instructions for the Thermo Fisher microplate reader (Thermo Fisher Scientific, USA).

Lipid peroxidation and protein carbonylation assays. Lipid peroxidation and protein carbonylation were assessed by determining the amount of malondialdehyde (MDA) adducts that formed with 2-thiobarbituric acid or carbonyls in proteins in tissue extracts using a Lipid Peroxidation (MDA) Assay Kit (Abcam, ab118970) and Protein Carbonyl Content Assay Kit (Abcam, ab126287), respectively, according to the manufacturer's instructions for the Thermo Fisher microplate reader (Thermo Fisher Scientific, USA).

Levels of total glutathione and the ratio of reduced to oxidized glutathione. In tissue extracts, the levels of total glutathione and the ratio of reduced to oxidized glutathione were

measured with a GSH/GSSG Ratio Detection Assay Kit (Abcam, ab138881) on a Cary Eclipse fluorescence spectrophotometer (Agilent Technologies, USA).

Confocal microscopy. On the day before the experiment, liver fibroblasts were seeded into 35-mm glass-bottom dishes (MatTek) with 14-mm glass microwells. For mitochondrial staining, MitoTracker Deep Red FM (Thermo Fisher) was diluted in dimethyl sulfoxide (according to the manufacturer's instructions) to obtain a final concentration of 25 nM. After staining, cells were fixed with 4% formaldehyde prepared in isotonic phosphate-buffered saline (PBS) and washed twice (5 min) with the same buffer. Permeabilization was achieved by incubating cells with PBS containing 0.05% Tween-20 and 0.1% Triton X-100 for 10 min at room temperature. The cells were washed twice (5 min) with PBS containing 0.2% Tween-20 and incubated with 1% bovine serum albumin (BSA) for 1 h on an orbital shaker to prevent the nonspecific binding of antibodies. Primary antibodies (anti-Hexokinase 1, ab55144, and anti-Hexokinase II, ab76959, Abcam) diluted 1:1000 in PBS containing 1% BSA were incubated with cells for 16 h at 4°C with constant gentle shaking on an orbital shaker. Cells were washed twice (5 min) with PBS containing 0.2% Tween-20 and incubated with a secondary antibody (Alexa Fluor 488-conjugated goat anti-mouse IgG, Life Technologies, A11001) diluted 1:5000 for 1 h at room temperature with shaking. "Fluoromount" medium containing DAPI (Invitrogen) was used to mount the glass slides. Cells were analyzed using a Carl Zeiss LSM700 confocal laser microscope equipped with a 63X objective in Opti-Mem without phenol red at room temperature (excitation/emission wavelengths 480/520 for Alexa Fluor 488 and 610/690 for MitoTracker Deep Red FM). The overlapping coefficient for red and green fluorescence was calculated using Zen software (Zeiss, Germany).

Statistics. Data are presented as the mean ± standard deviation (SD) or standard error of the mean (SEM). The Shapiro-Wilcoxon normality test was used to estimate the distribution within groups. One-way analysis of variance (ANOVA) followed by Tukey's post hoc test was used to identify differences among multiple groups of animals and ages with normal distribution. To calculate significant differences for non-normal distributions of the mentioned groups, we used one-way Kruskal-Wallis nonparametric ANOVA followed by the post hoc Dunn test. All calculations were performed using Prism 7.0 software (GraphPad, USA) and Website VassarStats for Statistical Computation (www.vassarstats.net). A P-value <0.05 (#) was considered significant and was indicative of the differences in comparison to the control. All marks presented in the figures related to the calculated significance: * P-value <0.01, ** <0.001 and *** <0.0001.

References

1. Bessman SP (1954) A contribution to the mechanism of diabetes mellitus. *Fat metabolism*, ed Najjar WA (Johns Hopkins Press, Homewood, Md), pp 133-137.
2. Arora KK & Pedersen PL (1988) Functional significance of mitochondrial bound hexokinase in tumor cell metabolism. Evidence for preferential phosphorylation of glucose by intramitochondrially generated ATP. *J Biol Chem* 263(33):17422-17428.
3. Il'in VS, Pleskov VM, & Razumovskaia NI (1967) [Hexokinase from the soluble fraction and mitochondria of skeletal muscles, embryo, intact and denervated muscles from adult rabbits]. *Biokhimiya* 32(4):807-811 (Russ).
4. Reid S & Masters C (1985) On the developmental properties and tissue interactions of hexokinase. *Mech Ageing Dev* 31(2):197-212.
5. BeltrandelRio H & Wilson JE (1991) Hexokinase of rat brain mitochondria: relative importance of adenylate kinase and oxidative phosphorylation as sources of substrate ATP, and interaction with intramitochondrial compartments of ATP and ADP. *Arch Biochem Biophys* 286(1):183-194.
6. Viitanen PV, Geiger PJ, Ericksonviitanen S, & Bessman SP (1984) Evidence for functional hexokinase compartmentation in rat skeletal-muscle mitochondria. *J Biol Chem* 259(15):9679-9686.
7. Perevoshchikova IV, Zorov SD, Kotova EA, Zorov DB, & Antonenko YN (2010) Hexokinase inhibits flux of fluorescently labeled ATP through mitochondrial outer membrane porin. *FEBS letters* 584(11):2397-2402.
8. Mitchell P (1961) Coupling of phosphorylation to electron and hydrogen transfer by a chemi-osmotic type of mechanism. *Nature* 191:144-148.
9. Liberman EA, Topaly VP, Tsofina LM, Jasaitis AA, & Skulachev VP (1969) Mechanism of coupling of oxidative phosphorylation and the membrane potential of mitochondria. *Nature* 222(5198):1076-1078.
10. Loschen G, Flohe L, & Chance B (1971) Respiratory chain linked H_2O_2 production in pigeon heart mitochondria. *FEBS letters* 18(2):261-&.
11. Boveris A, Chance B, & Oshino N (1972) Cellular production of hydrogen-peroxide. *Biochem J* 128(3):617-&.
12. Korshunov SS, Skulachev VP, & Starkov AA (1997) High protonic potential actuates a mechanism of production of reactive oxygen species in mitochondria. *FEBS letters* 416(1):15-18.

13. da-Silva WS, *et al*. (2004) Mitochondrial bound hexokinase activity as a preventive antioxidant defense: steady-state ADP formation as a regulatory mechanism of membrane potential and reactive oxygen species generation in mitochondria. *J Biol Chem* 279(38):39846-39855.
14. Meyer LE, *et al*. (2006) Mitochondrial creatine kinase activity prevents reactive oxygen species generation: antioxidant role of mitochondrial kinase-dependent ADP re-cycling activity. *J Biol Chem* 281(49):37361-37371.
15. Santiago AP, Chaves EA, Oliveira MF, & Galina A (2008) Reactive oxygen species generation is modulated by mitochondrial kinases: correlation with mitochondrial antioxidant peroxidases in rat tissues. *Biochimie* 90(10):1566-1577.
16. Tannahill GM, *et al*. (2013) Succinate is an inflammatory signal that induces IL-1beta through HIF-1alpha. *Nature* 496(7444):238-242.
17. Murphy MP & O'Neill LAJ (2018) Krebs cycle reimagined: the emerging roles of succinate and itaconate as signal transducers. *Cell* 174(4):780-784.
18. Michelucci A, *et al*. (2013) Immune-responsive gene 1 protein links metabolism to immunity by catalyzing itaconic acid production. *Proc Natl Acad Sci U S A* 110(19):7820-7825.
19. Chouchani ET, *et al*. (2014) Ischaemic accumulation of succinate controls reperfusion injury through mitochondrial ROS. *Nature* 515(7527):431-435.
20. Mills EL, *et al*. (2016) Succinate dehydrogenase supports metabolic repurposing of mitochondria to drive inflammatory macrophages. *Cell* 167(2):457-470 e413.
21. Skulachev VP, Bogachev AV, & Kasparinsky FO (2013) *Principles of bioenergetics* (Springer Berlin Heidelberg).
22. Park TJ, *et al*. (2017) Fructose-driven glycolysis supports anoxia resistance in the naked mole-rat. *Science* 356(6335):305-308.
23. Browe BM, Vice EN, & Park TJ (2018) Naked Mole-Rats: Blind, Naked, and Feeling No Pain. *Anat Rec (Hoboken)*.
24. Nemat-Gorgani M & Wilson JE (1980) Ambiquitous behavior--a biological phenomenon of general significance? *Curr Top Cell Regul* 16:45-54.
25. Wilson JE (1985) Regulation of mammalian hexokinase activity. *Regulation of Carbohydrate Metabolism*, ed Beitner R (CRC Press, Inc, Boca Raton), Vol I, pp 45-85.
26. Muller AP, *et al*. (2013) Insulin prevents mitochondrial generation of H_2O_2 in rat brain. *Exp Neurol* 247:66-72.
27. Frolkis VV (1988) *Aging and an increase in longevity* (Nauka, Leningrad).

28. Skulachev MV & Skulachev VP (2017) Programmed aging of mammals: proof of concept and prospects of biochemical approaches for anti-aging therapy. *Biochemistry (Mosc)* 82(12):1403-1422.
29. Weismann A (1889) *Essays upon heredity and kindred biological problems* (Clarendon press, Oxford) 2d Ed.
30. Kerr JF, Wyllie AH, & Currie AR (1972) Apoptosis: a basic biological phenomenon with wide-ranging implications in tissue kinetics. *Br J Cancer* 26(4):239-257.
31. Pozniakovsky AI, *et al*. (2005) Role of mitochondria in the pheromone- and amiodarone-induced programmed death of yeast. *J Cell Biol* 168(2):257-269.
32. Skulachev VP (1997) Aging is a specific biological function rather than the result of a disorder in complex living systems: Biochemical evidence in support of Weismann's hypothesis. *Biochemistry (Mosc)* 62(11):1191-1195.
33. Skulachev VP (2003) Aging and the programmed death phenomena. *Topics Curr Genet, Model Systems in Aging*, ed Nystrom T, Osiewacz, H. D. (Springer, Berlin Heidelberg), Vol 3, pp 192-237.
34. Skulachev VP (2012) What is "phenoptosis" and how to fight it? *Biochemistry (Mosc)* 77(7):689-706.
35. Skulachev VP & Lyamzaev KG (2019) Aging as phenoptotic phenomenon. *Encyclopedia of Gerontology and Population Aging*, eds Gu D & Dupre ME (Springer, Cham), pp 1-4.
36. Ezcurra M, *et al*. (2018) *C. elegans* eats its own intestine to make yolk leading to multiple senescent pathologies. *Curr Biol* 28(20):3352-3352.
37. Lohr JN, Galimov ER, & Gems D (2019) Does senescence promote fitness in Caenorhabditis elegans by causing death? *Ageing Res Rev* 50:58-71.
38. Li J, Labbadia J, & Morimoto RI (2017) Rethinking HSF1 in stress, development, and organismal health. *Trends Cell Biol* 27(12):895-905.
39. Labbadia J, *et al*. (2017) Mitochondrial stress restores the heat shock response and prevents proteostasis collapse during aging. *Cell Rep* 21(6):1481-1494.
40. Skulachev VP, *et al*. (2017) Neoteny, prolongation of youth: from naked mole rats to "naked apes" (humans). *Physiol Rev* 97(2):699-720.
41. Holtze S, *et al*. (2016) Study of age-dependent structural and functional changes of mitochondria in skeletal muscles and heart of naked mole rats (*Heterocephalus glaber*). *Biochemistry (Mosc)* 81(12):1429-1437.
42. Schmalhausen II (1949) *Factors of evolution: the theory of stabilizing selection*. (Blakiston, Philadelphia).

43. Levit GS, Hossfeld U, & Olsson L (2006) From the "Modern Synthesis" to cybernetics: Ivan Ivanovich Schmalhausen (1884-1963) and his research program for a synthesis of evolutionary and developmental biology. *Journal of experimental zoology. Part B, Molecular and developmental evolution* 306(2):89-106.
44. Miller CJ, *et al*. (2012) Disruption of Nrf2/ARE signaling impairs antioxidant mechanisms and promotes cell degradation pathways in aged skeletal muscle. *Biochim Biophys Acta* 1822(6):1038-1050.
45. Li N, Muthusamy S, Liang R, Sarojini H, & Wang E (2011) Increased expression of miR-34a and miR-93 in rat liver during aging, and their impact on the expression of Mgst1 and Sirt1. *Mech Ageing Dev* 132(3):75-85.
46. Suh JH, *et al*. (2004) Decline in transcriptional activity of Nrf2 causes age-related loss of glutathione synthesis, which is reversible with lipoic acid. *Proc Natl Acad Sci U S A* 101(10):3381-3386.
47. Duan W, *et al*. (2009) Nrf2 activity is lost in the spinal cord and its astrocytes of aged mice. *In Vitro Cell Dev Biol Anim* 45(7):388-397.
48. Tonelli C, Chio IIC, & Tuveson DA (2018) Transcriptional regulation by Nrf2. *Antioxid Redox Signal* 29(17):1727-1745.
49. Lewis KN, *et al*. (2015) Regulation of Nrf2 signaling and longevity in naturally long-lived rodents. *Proc Natl Acad Sci U S A* 112(12):3722-3727.
50. Zhou Y, Wu H, Zhao M, Chang C, & Lu Q (2016) The bach family of transcription factors: a comprehensive review. *Clin Rev Allergy Immunol* 50(3):345-356.
51. de-Souza-Ferreira E, Rios-Neto IM, Martins EL, & Galina A (2019) Mitochondria-coupled glucose phosphorylation develops after birth to modulate H_2O_2 release and calcium handling in rat brain. *J Neurochem* 149(5):624-640.
52. Migliaccio E, *et al*. (1999) The p66shc adaptor protein controls oxidative stress response and life span in mammals. *Nature* 402(6759):309-313.
53. Napoli C, *et al*. (2003) Deletion of the p66Shc longevity gene reduces systemic and tissue oxidative stress, vascular cell apoptosis, and early atherogenesis in mice fed a high-fat diet. *Proc Natl Acad Sci U S A* 100(4):2112-2116.
54. Giorgio M, *et al*. (2004) p66Shc is a signal transduction redox enzyme. *Biochim Biophys Acta* 1658:55-55.
55. Maurel A, *et al*. (2003) Age-dependent increase in hydrogen peroxide production by cardiac monoamine oxidase A in rats. *American journal of physiology. Heart and circulatory physiology* 284(4):H1460-1467.

56. Grivennikova VG, Kareyeva AV, & Vinogradov AD (2010) What are the sources of hydrogen peroxide production by heart mitochondria? *Biochim Biophys Acta* 1797(6-7):939-944.
57. Smeele KMA, *et al*. (2011) Disruption of hexokinase II-mitochondrial binding blocks ischemic preconditioning and causes rapid cardiac necrosis. *Circ Res* 108(10):1165-U1134.
58. Wu RX, *et al*. (2012) Hexokinase II knockdown results in exaggerated cardiac hypertrophy via increased ROS production. *Embo Mol Med* 4(7):633-646.
59. Ong SG, *et al*. (2014) HIF-1 reduces ischaemia-reperfusion injury in the heart by targeting the mitochondrial permeability transition pore. *Cardiovasc Res* 104(1):24-36.
60. Camacho-Pereira J, Meyer LE, Machado LB, Oliveira MF, & Galina A (2009) Reactive oxygen species production by potato tuber mitochondria is modulated by mitochondrially bound hexokinase activity. *Plant Physiol* 149(2):1099-1110.
61. Saraiva LM, *et al*. (2010) Amyloid-beta triggers the release of neuronal hexokinase 1 from mitochondria. *PLoS One* 5(12):e15230.
62. Kraupp O, Adler-Kastner L, Niessner H, & Plank B (1967) The effects of starvation and of acute and chronic alloxan diabetes on myocardial substrate levels and on liver glycogen in the rat in vivo. *Eur J Biochem* 2(2):197-214.
63. Kraupp O, Adlerkas.L, Niessner H, & Plank B (1968) A correlation study between myocardial substrate levels and blood glucose level in normal and in acute and chronic alloxan-diabetic rats *in vivo*. *Eur J Biochem* 4(2):164-172.
64. Harman D (1972) The biologic clock: the mitochondria? *J Am Ger Soc* 20(4):145-147.
65. Munro D, Baldy C, Pamenter ME, & Treberg JR (2019) The exceptional longevity of the naked mole-rat may be explained by mitochondrial antioxidant defenses. *Aging Cell* 18(3):e12916.
66. Labinskyy N, *et al*. (2006) Comparison of endothelial function, $O_2^{\bullet-}$ and H_2O_2 production, and vascular oxidative stress resistance between the longest-living rodent, the naked mole rat, and mice. *Am J Physiol-Heart C* 291(6):H2698-H2704.
67. Dilman VM (1978) Ageing, metabolic immunodepression and carcinogenesis. *Mech Ageing Dev* 8(3):153-173.
68. Comfort A (1979) *The biology of senescence, 3rd ed* (Elsevier, New York).
69. Tepp K, *et al*. (2017) Changes in the mitochondrial function and in the efficiency of energy transfer pathways during cardiomyocyte aging. *Mol Cell Biochem* 432(1-2):141-158.

70. Bohn JA, *et al*. (2018) Identification of diverse target RNAs that are functionally regulated by human Pumilio proteins. *Nucleic Acids Res* 46(1):362-386.
71. D'Amico D, *et al*. (2019) The RNA-binding protein PUM2 impairs mitochondrial dynamics and mitophagy during aging. *Mol Cell* 73(4):775-787.
72. Kopp F, *et al*. (2019) PUMILIO hyperactivity drives premature aging of Norad-deficient mice. *Elife* 8.
73. Nederlof R, *et al*. (2017) Reducing mitochondrial bound hexokinase II mediates transition from non-injurious into injurious ischemia/reperfusion of the intact heart. *J Physiol Biochem* 73(3):323-333.
74. Pantic B, *et al*. (2013) Myotonic dystrophy protein kinase (DMPK) prevents ROS-induced cell death by assembling a hexokinase II-Src complex on the mitochondrial surface. *Cell Death Dis* 4:e858.
75. Gottlob K, *et al*. (2001) Inhibition of early apoptotic events by Akt/PKB is dependent on the first committed step of glycolysis and mitochondrial hexokinase. *Gene Dev* 15(11):1406-1418.
76. Miyamoto S, Murphy AN, & Brown JH (2008) Akt mediates mitochondrial protection in cardiomyocytes through phosphorylation of mitochondrial hexokinase-II. *Cell Death Differ* 15(3):521-529.
77. Zhou YX, *et al*. (2015) FV-429 induced apoptosis through ROS-mediated ERK2 nuclear translocation and p53 activation in gastric cancer cells. *J Cell Biochem* 116(8):1624-1637.
78. Stiles BL (2009) PI-3-K and AKT: onto the mitochondria. *Adv Drug Deliver Rev* 61(14):1276-1282.
79. Nyquist-Battie C & Freter M (1988) Cardiac mitochondrial abnormalities in a mouse model of the fetal alcohol syndrome. *Alcohol Clin Exp Res* 12(2):264-267.
80. Figueira TR, Melo DR, Vercesi AE, & Castilho RF (2012) Safranine as a fluorescent probe for the evaluation of mitochondrial membrane potential in isolated organelles and permeabilized cells. *Methods Mol Biol* 810:103-117.
81. Vyssokikh MY, *et al*. (2001) Adenine nucleotide translocator isoforms 1 and 2 are differently distributed in the mitochondrial inner membrane and have distinct affinities to cyclophilin D. *Biochem J* 358:349-358.
82. Antonenko YN, *et al*. (2008) Mitochondria-targeted plastoquinone derivatives as tools to interrupt execution of the aging program. 1. Cationic plastoquinone derivatives: Synthesis and *in vitro* studies. *Biochemistry (Mosc)* 73(12):1273-1287.
83. Scheer WD, Lehmann HP, & Beeler MF (1978) An improved assay for hexokinase activity in human tissue homogenates. *Anal Biochem* 91(2):451-463.

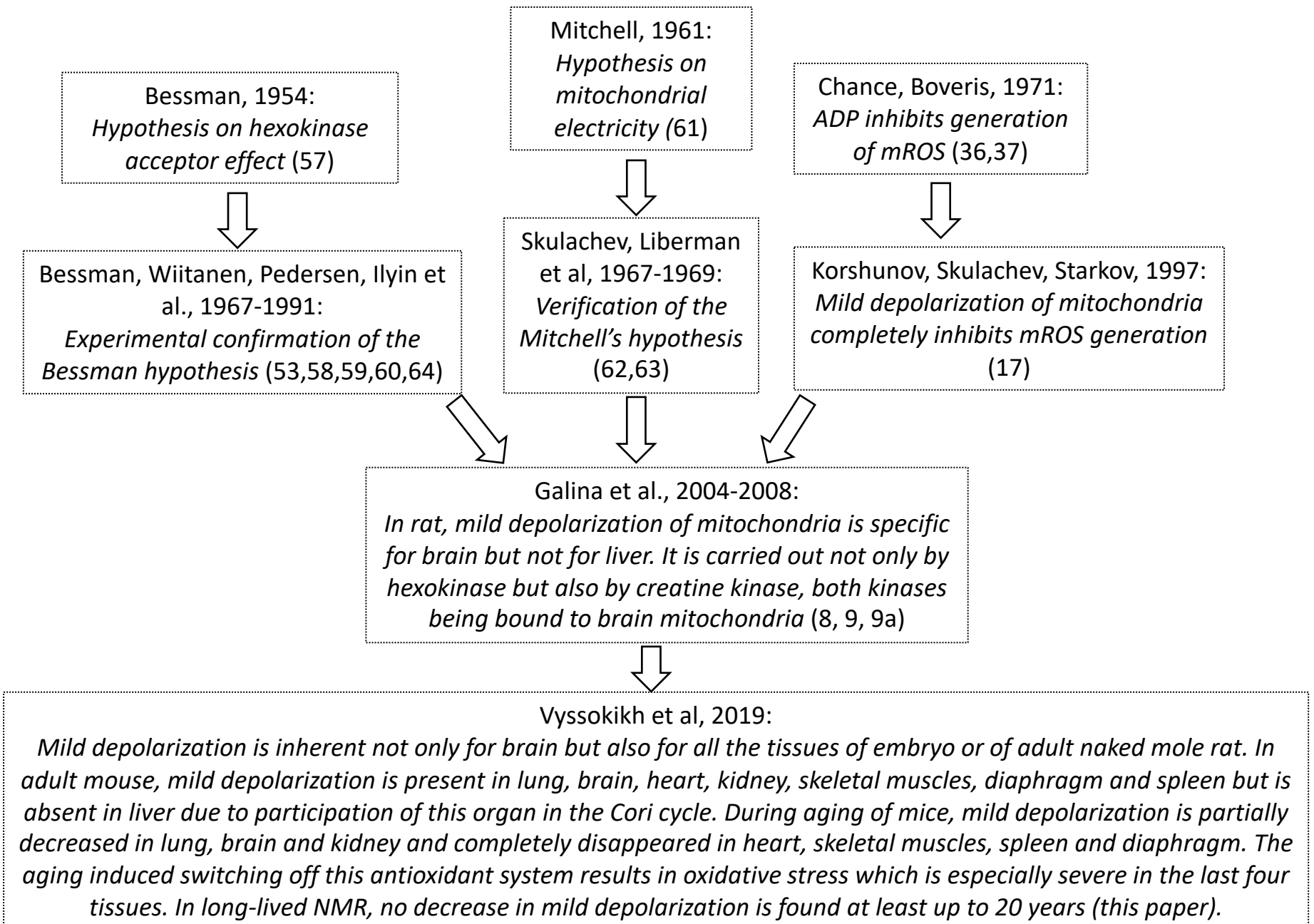

Fig. S1. History of the discovery of mild depolarization.

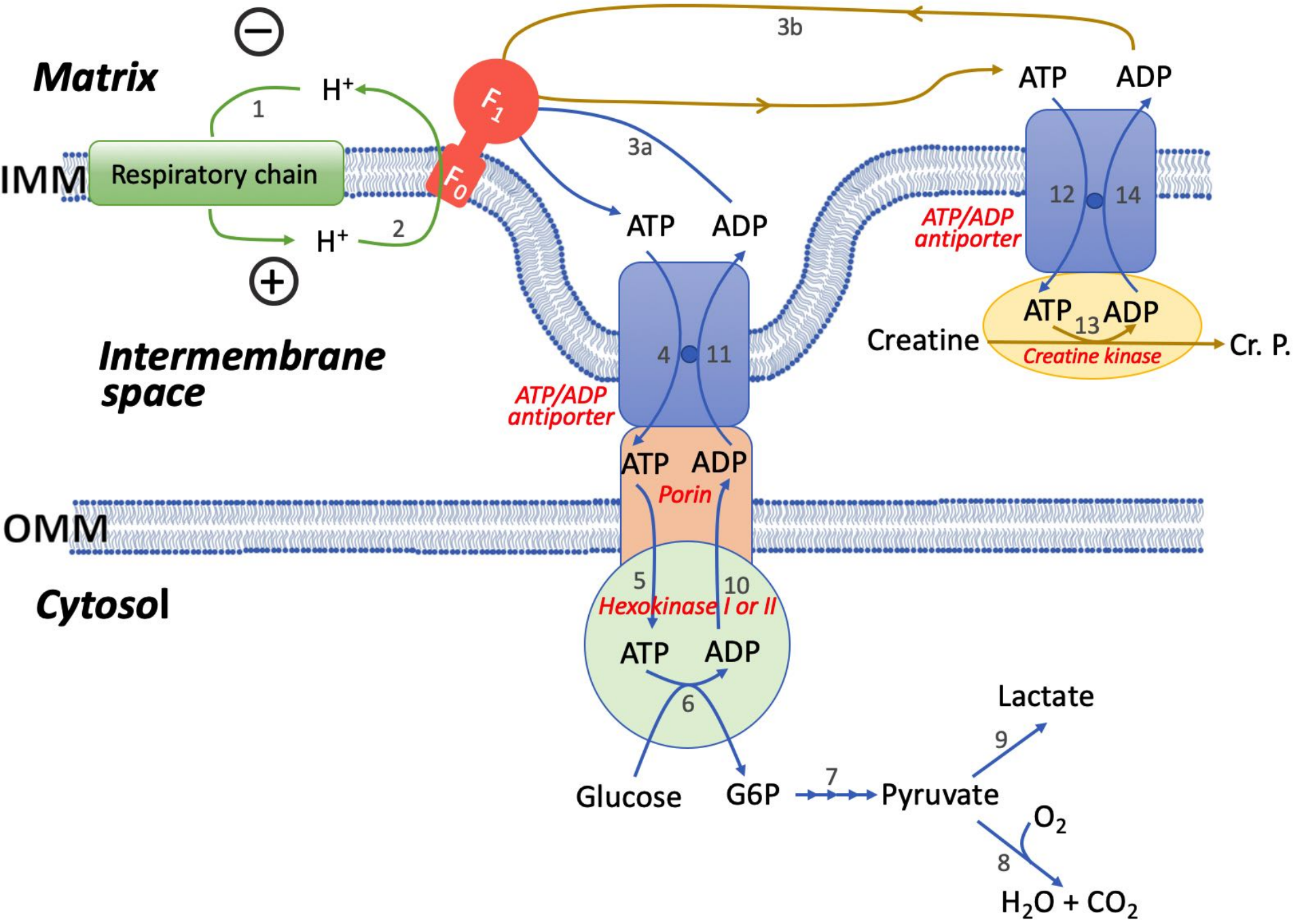

Fig. S2. Intracellular locations of components of mild depolarization. IMM, inner mitochondrial membrane. OMM, outer mitochondrial membrane. (1) Complexes I, III and IV produce an electrochemical potential of H^+ ions ($\Delta\bar{\mu}_{H}^{+}$) on the IMM. In mitochondria, $\Delta\bar{\mu}_{H}^{+}$ is presented by $\Delta\psi$ and ΔpH, with $\Delta\psi$ dominating. Its decrease provides the main contribution to mild depolarization. ΔpH is rather small but sufficient as the driving force for the accumulation of inorganic phosphate in the matrix due to the function of the $H_2PO^-_4 + H^+$ symporter in the IMM. $H_2PO^-_4$ is required for ATP synthesis from ADP by F_0F_1 (Complex V). (2, 3a, and 3b) $\Delta\bar{\mu}_{H}^{+}$-driven import of H^+ via F_0 is used as an energy source for the synthesis of ATP from ADP. (3a and 3b) As a source of ADP, hexokinase or creatine kinase are used, respectively. (4) ATP generated by F_0F_1 is expelled from the matrix by the ATP^{4-}/ADP^{3-} antiporter in exchange for ADP moving in the opposite direction. Since ATP and ADP have four and three negative charges, respectively, the ATP/ADP exchange is equivalent to the electrophoretic translocation of one negative charge from the matrix. (5) ATP transported by the antiporter crosses porin and interacts with the catalytic site of hexokinase I or II attached to porin. (6) Glucose is phosphorylated to G6P by hexokinase. (7) G6P initiates the glycolytic chain of reactions to form pyruvate. (8) Pyruvate is consumed by the Krebs cycle and respiratory chain to form H_2O and CO_2 from O_2 and electrons supplied by Complex IV (see Fig. 1). (9) If oxygen is unavailable, then pyruvate is converted to lactate. (10 and 11) ADP, the second hexokinase product, is transported by porin to the ATP/ADP antiporter which expels ADP to the matrix. (12 and 13) The transport of ATP to the catalytic side of creatine kinase induces creatine phosphorylation by ATP. (14) The resulting ADP is expelled to the matrix by the ATP/ADP antiporter. It is assumed that the distance between the inner and outer mitochondrial membranes is shortened in contact sites where the antiporter interacts with porin.

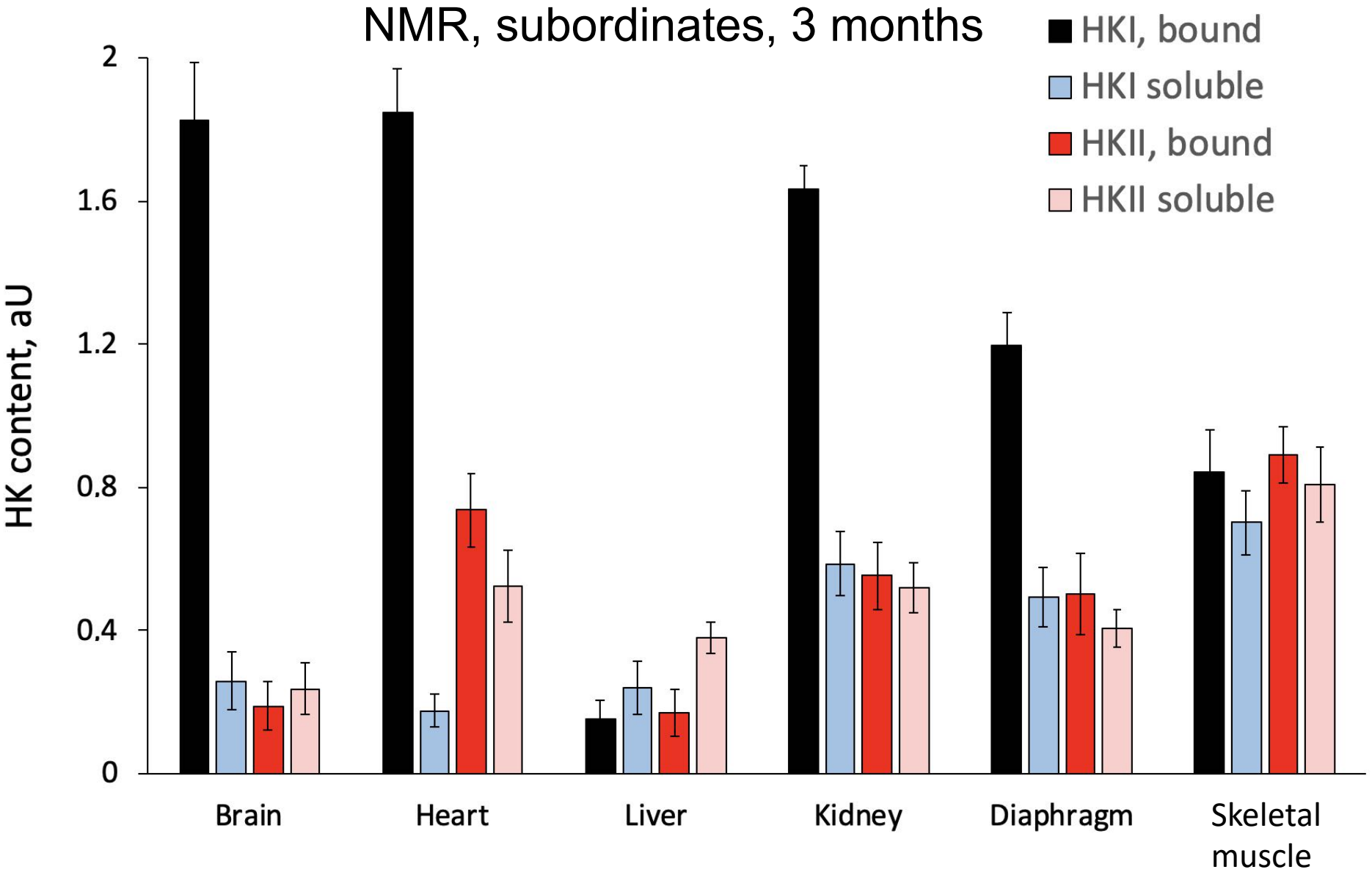

Fig. S3. Amounts of bound and soluble hexokinases I and II in different tissues from 3-month-old NMRs.

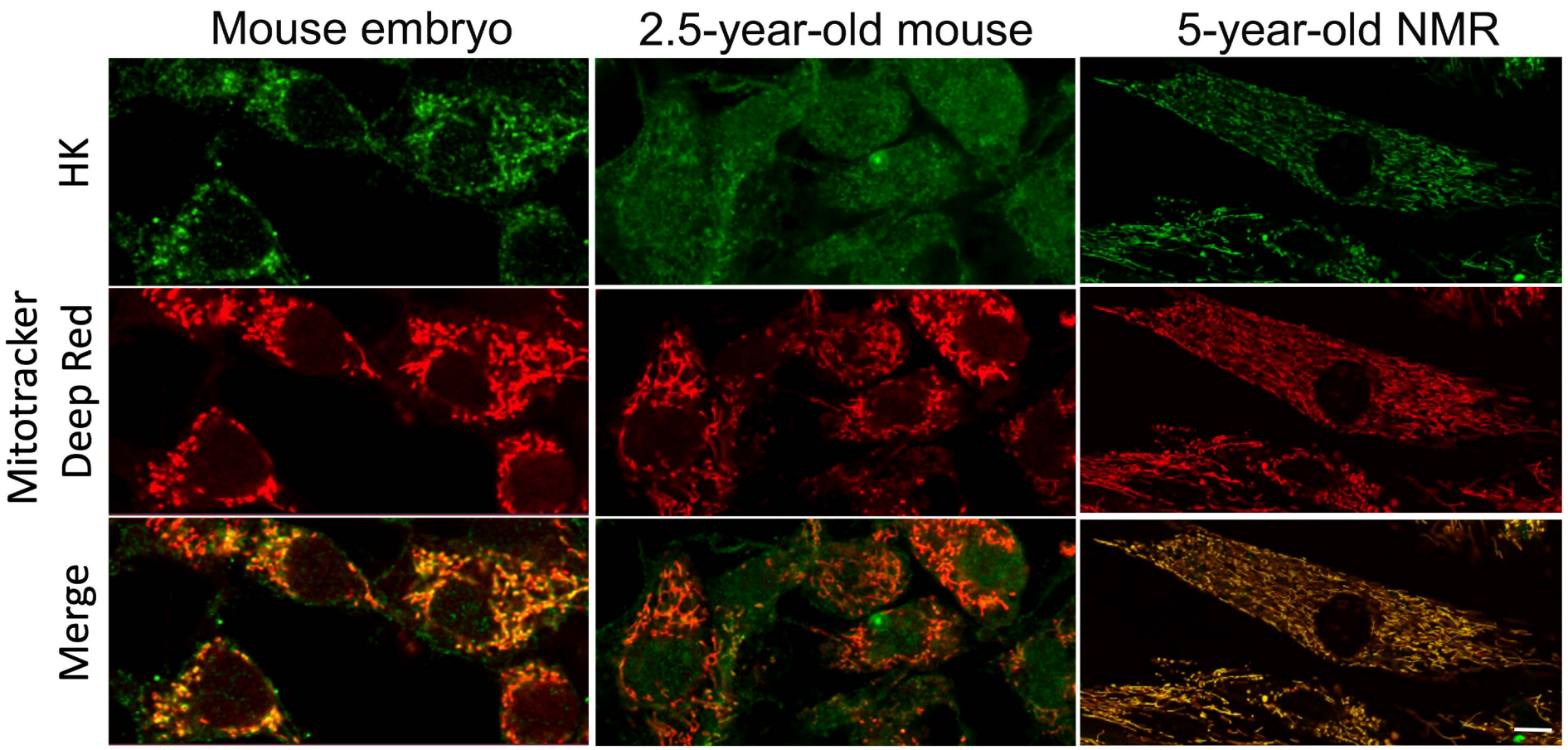

Fig. S4. Confocal microscopy of liver fibroblasts from mouse embryo, 2.5-year-old mouse and 5-year-old NMR subordinates.

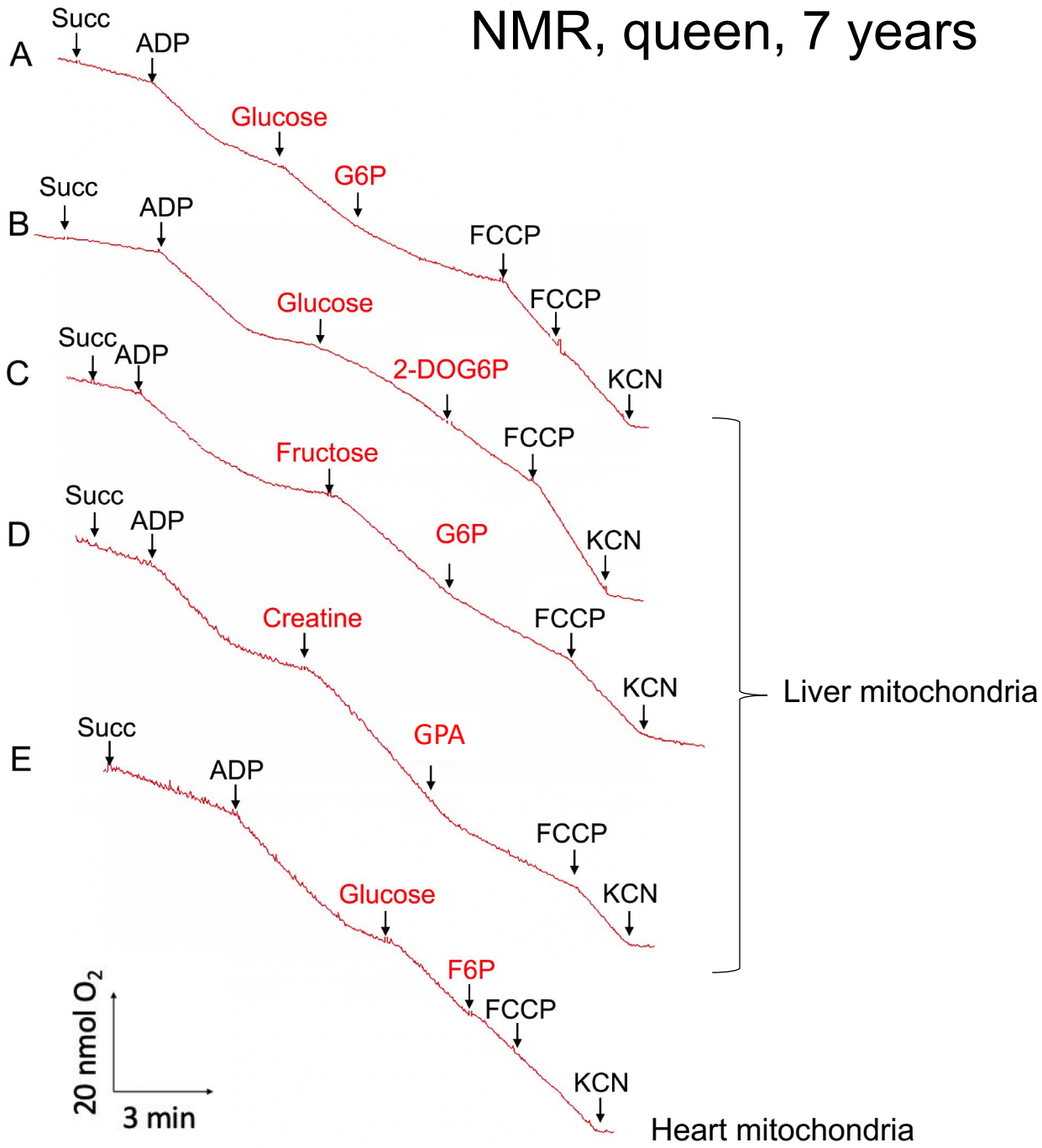

Fig. S5. Mitochondrial respiration in a 7-year-old NMR queen. The effects of some inhibitors and their analogs are shown. A-D, liver mitochondria. The following compounds were added at the indicated concentrations: 1 mM fructose-6-phosphate (F6P), 2 mM glucose, 1 mM G6P, 1 mM 2-deoxyglucose 6-phosphate (2DOG6P), 1 mM fructose, 3 mM creatine, and 250 mM guanidopropionic acid (GPA). E, Heart mitochondria. For conditions, see Fig. 3.

3 month mouse

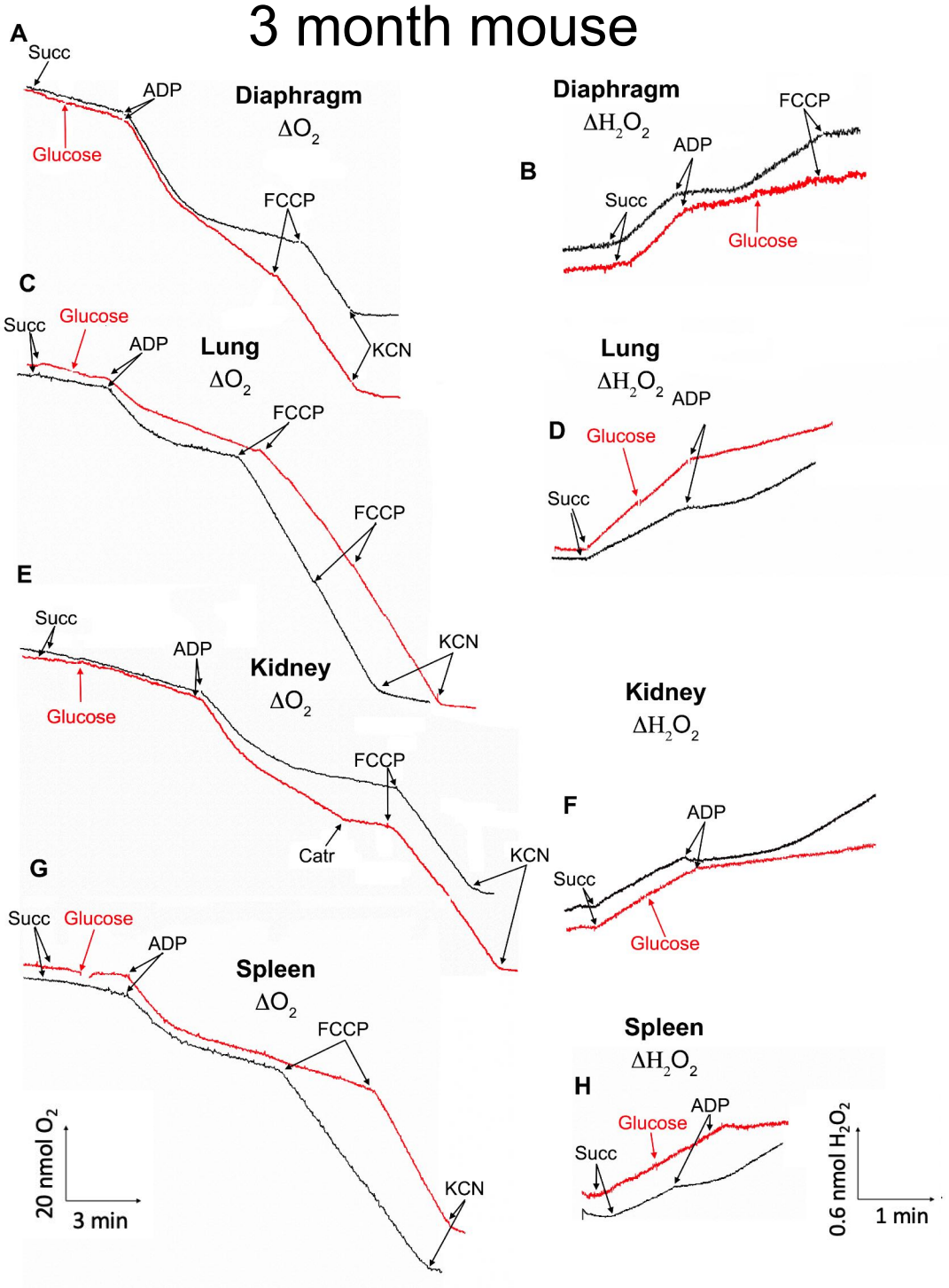

Fig. S6. Effects of glucose on State 4 respiration and H_2O_2 generation by mitochondria from different tissues of adult mice (Figs. 3A-F, continued).

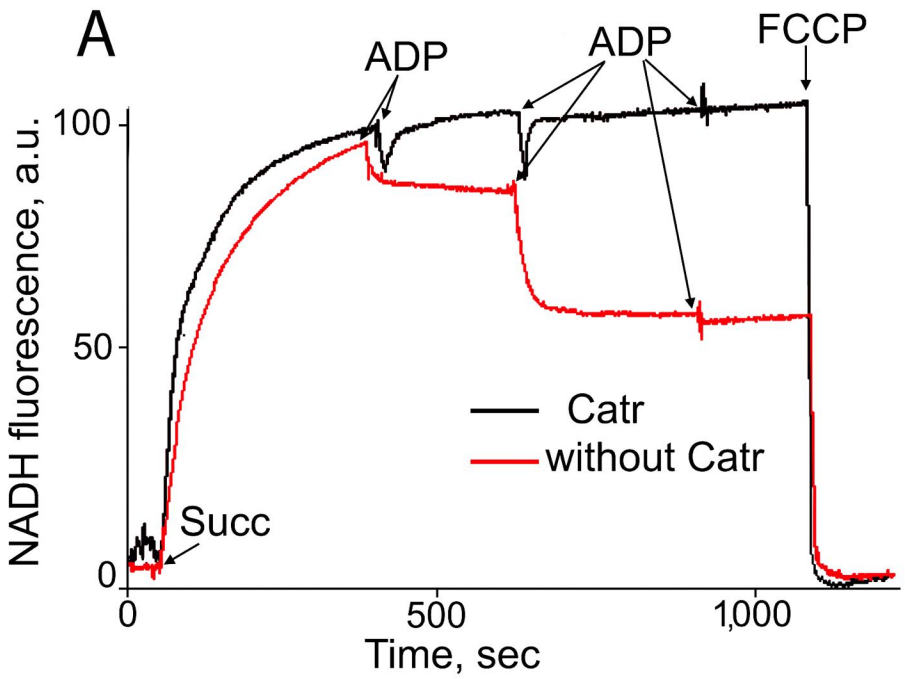

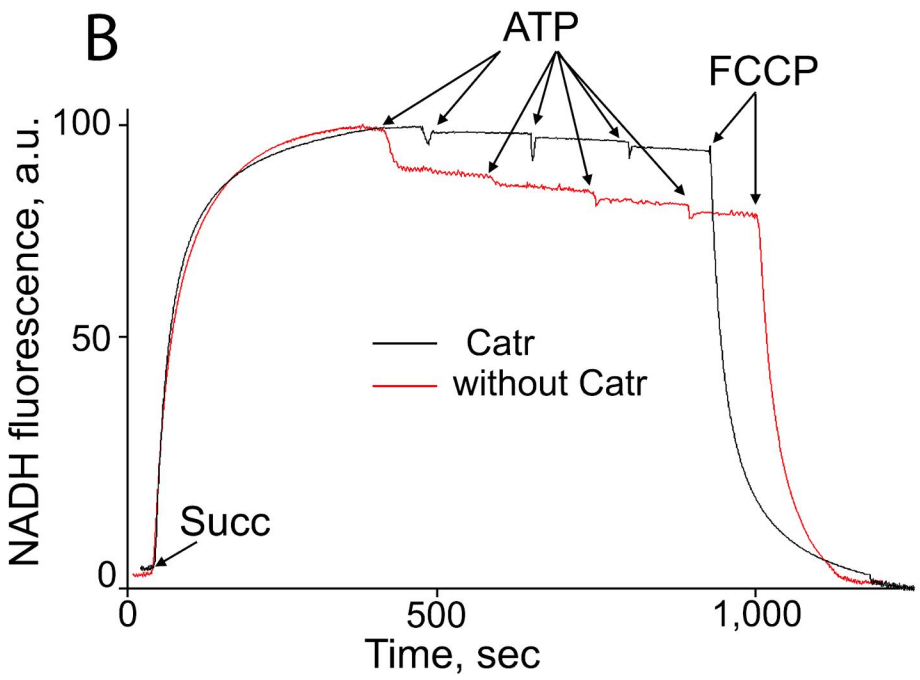

Fig. S7. Effects of ADP (A) and ATP (B) on reverse electron transfer from succinate to NAD^+ in the presence of oligomycin in adult mouse mitochondria. Each addition of nucleotide, 100 μM. Black or red curves, with or without Catr, respectively.

3 month mouse, heart

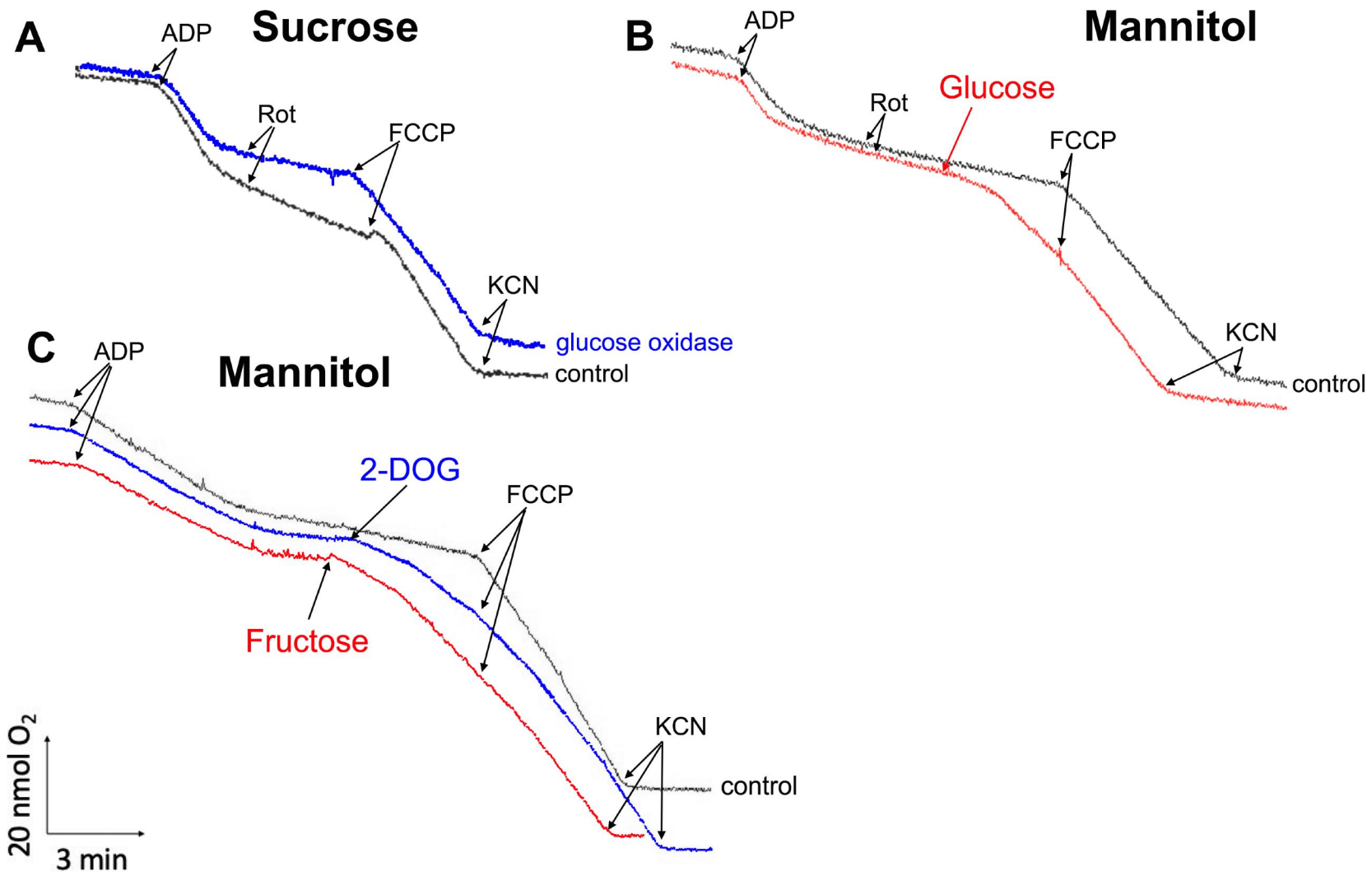

Fig. S8. Respiration of heart mitochondria (25 µg protein/mg) isolated from adult mice using sucrose (A) or mannitol (B and C). A, Mitochondria isolated in 250 mM sucrose, 0.5 mM EGTA, and 20 mM HEPES-NaOH, pH 7.6. No addition (control) *vs* a 10-min preincubation with 1 U glucose oxidase. B and C, Mitochondria isolated from the heart of adult mice in 300 mM mannitol, 0.5 mM EGTA, and 20 mM HEPES-NaOH, pH 7.6. No additions (control) *vs* 1 mM glucose. The following compounds were added: 100 µM ADP, 2 µM rotenone (rot), 10 nM FCCP, 1 mM KCN, 1 mM 2-DOG, and 3 mM fructose.

NMR, embryo

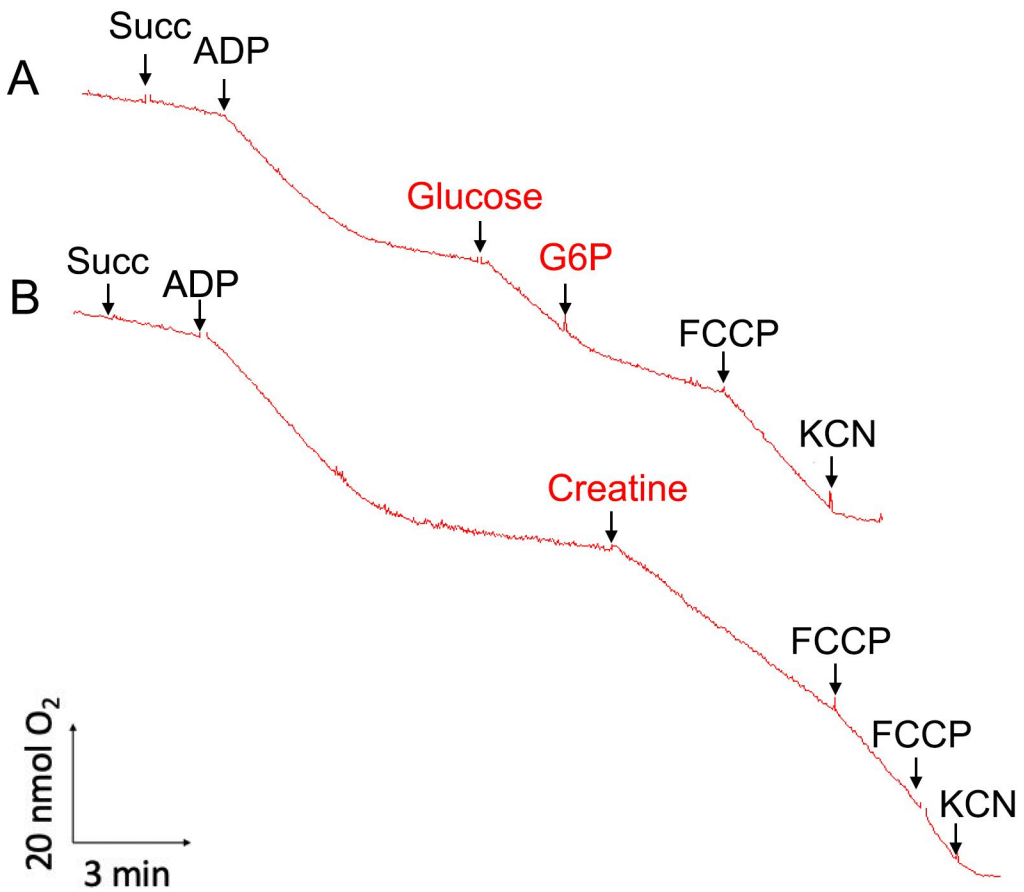

Fig. S9. Mitochondrial respiration in embryos of naked mole rats. The effects of glucose, G6P (A) and creatine (B) are shown.

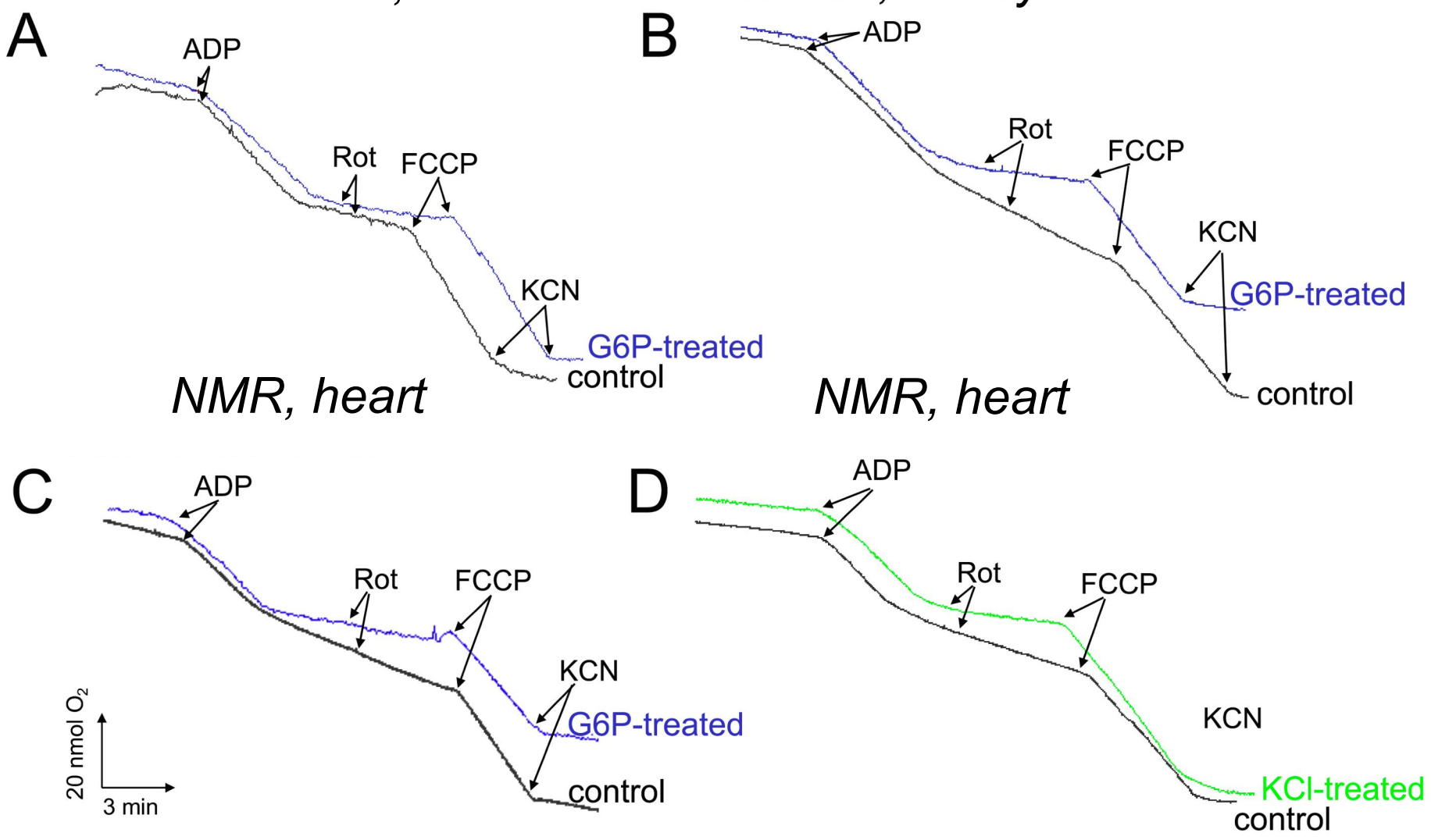

Fig. S10. Respiration of mitochondria from the heart of a 3-month-old-mouse, mouse embryo (18 days of embryogenesis) or NMR subordinate (3 years old), washed with a sucrose solution supplemented with or without 1 mM G6P or 300 mM KCl. For the other conditions, see Fig. 3.

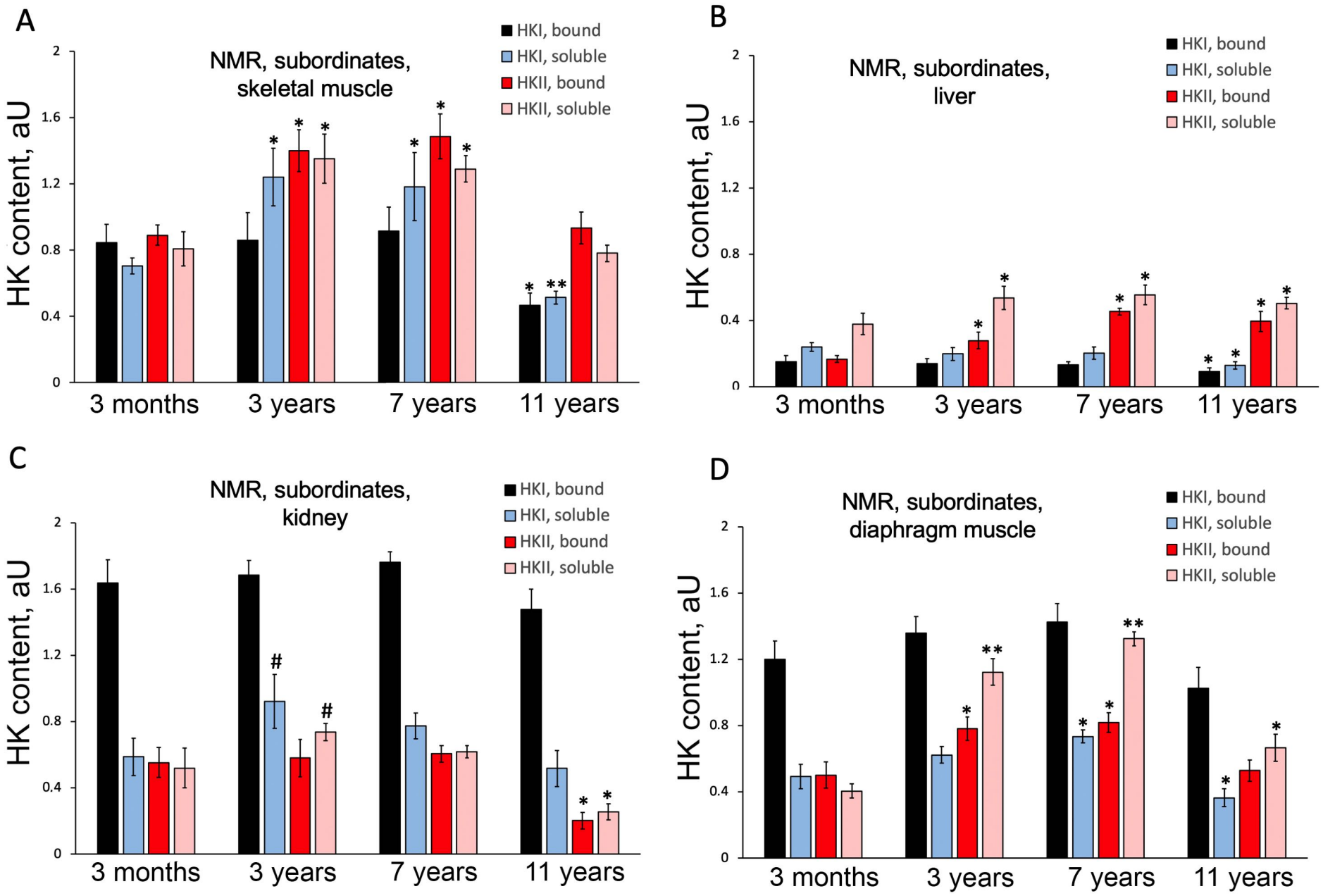

Fig. S11 A. Neoteny in naked mole rats: hexokinase II dominates over hexokinase I in skeletal muscle at the ages of 3-11 years but not at the age of 3 months. NMR subordinates. B-D, Dynamic changes in the levels of the two hexokinases in the liver, kidney and diaphragm from NMR subordinates; ages from 3 to 11 years. #, * and **, *p* values are <0.05, <0.01 and <0.001, respectively, for comparison of 3, 7, and 11 years NMR subordinates with 3 months NMR subordinates.

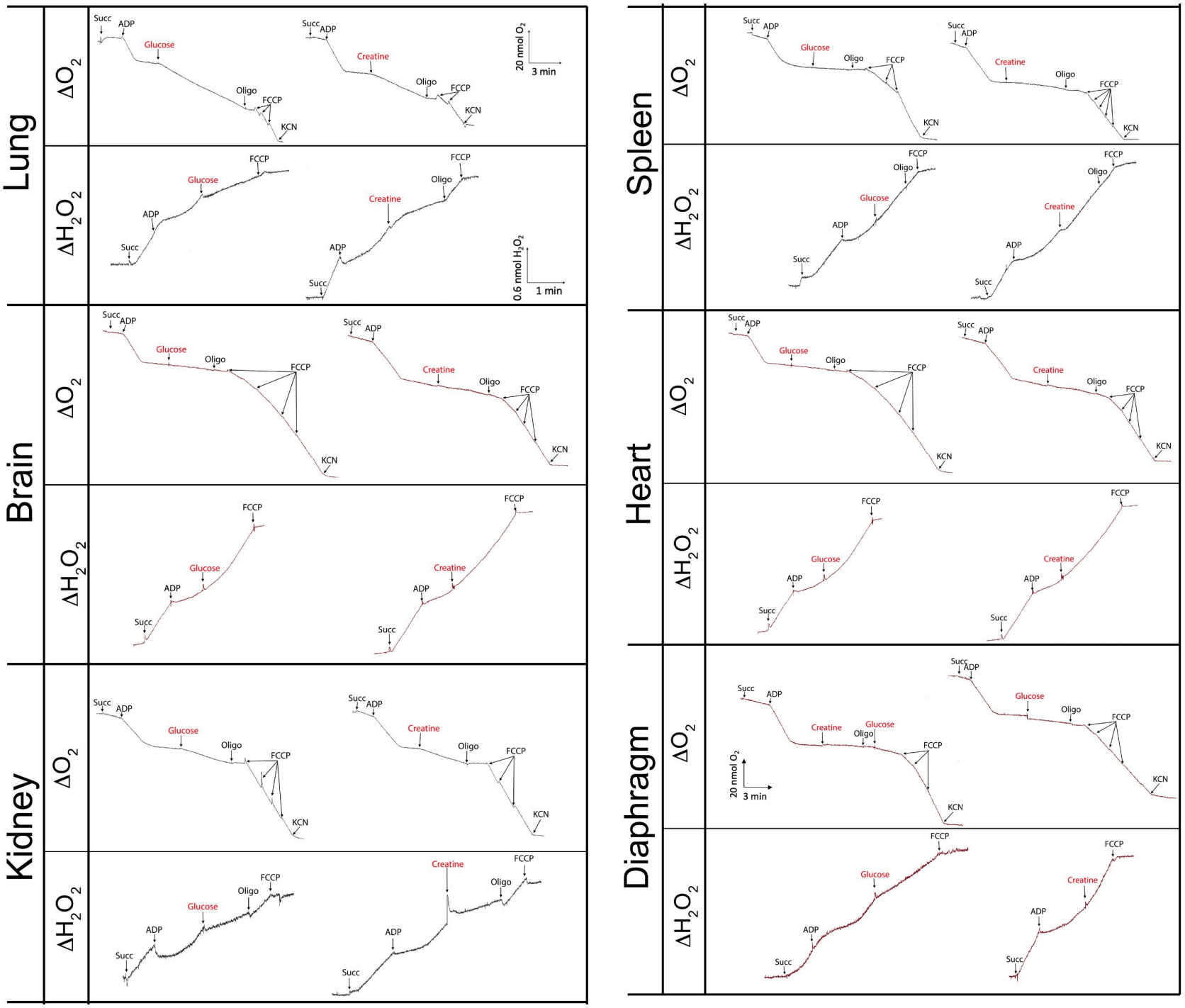

Fig. S12. Respiration and H_2O_2 generation by mitochondria isolated from different tissues from 2.5-year-old mice. For conditions, see Fig. 3.

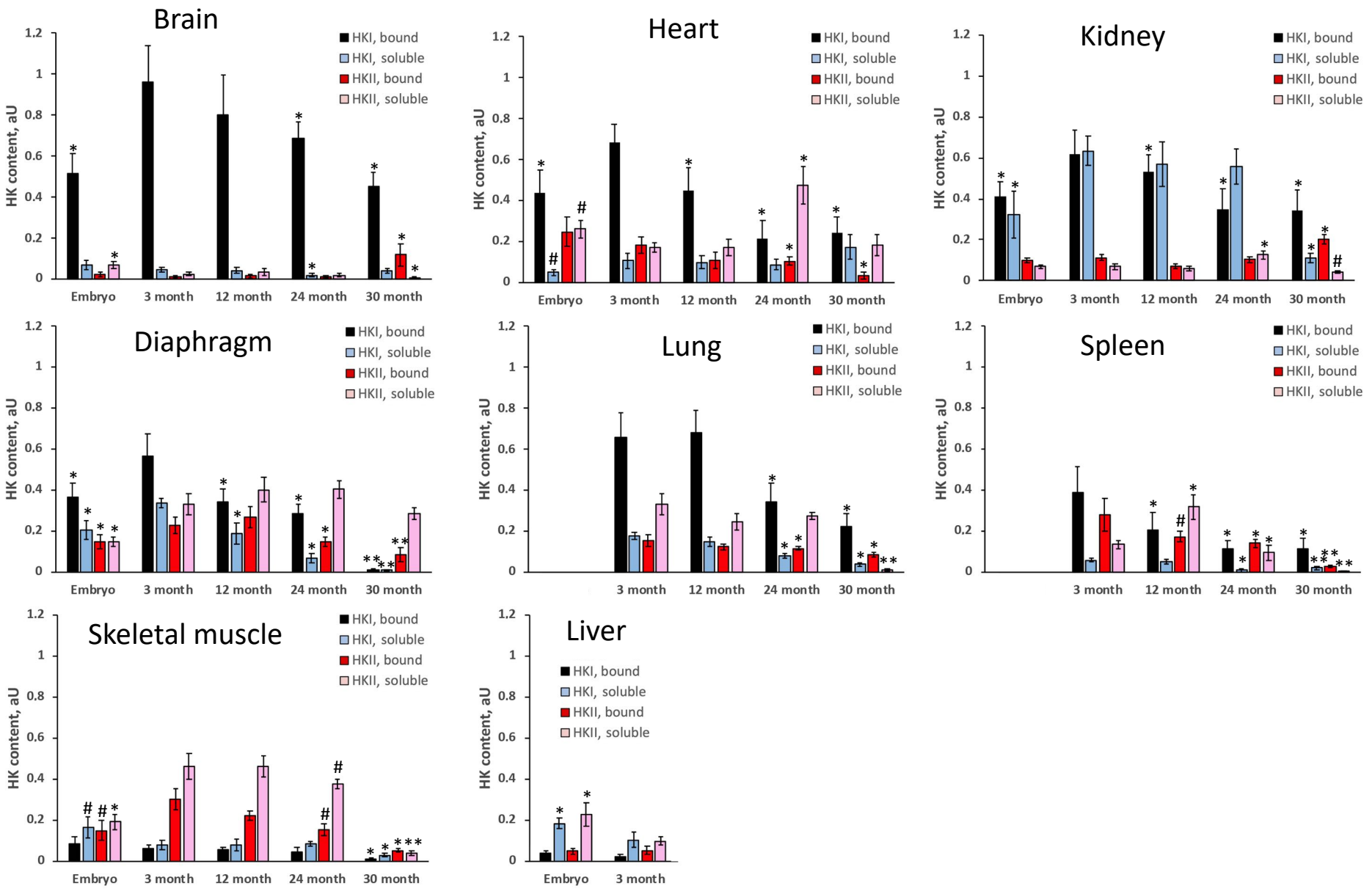

Fig. S13. The contents of mitochondria-bound hexokinases I and II from various tissues as a function of age.

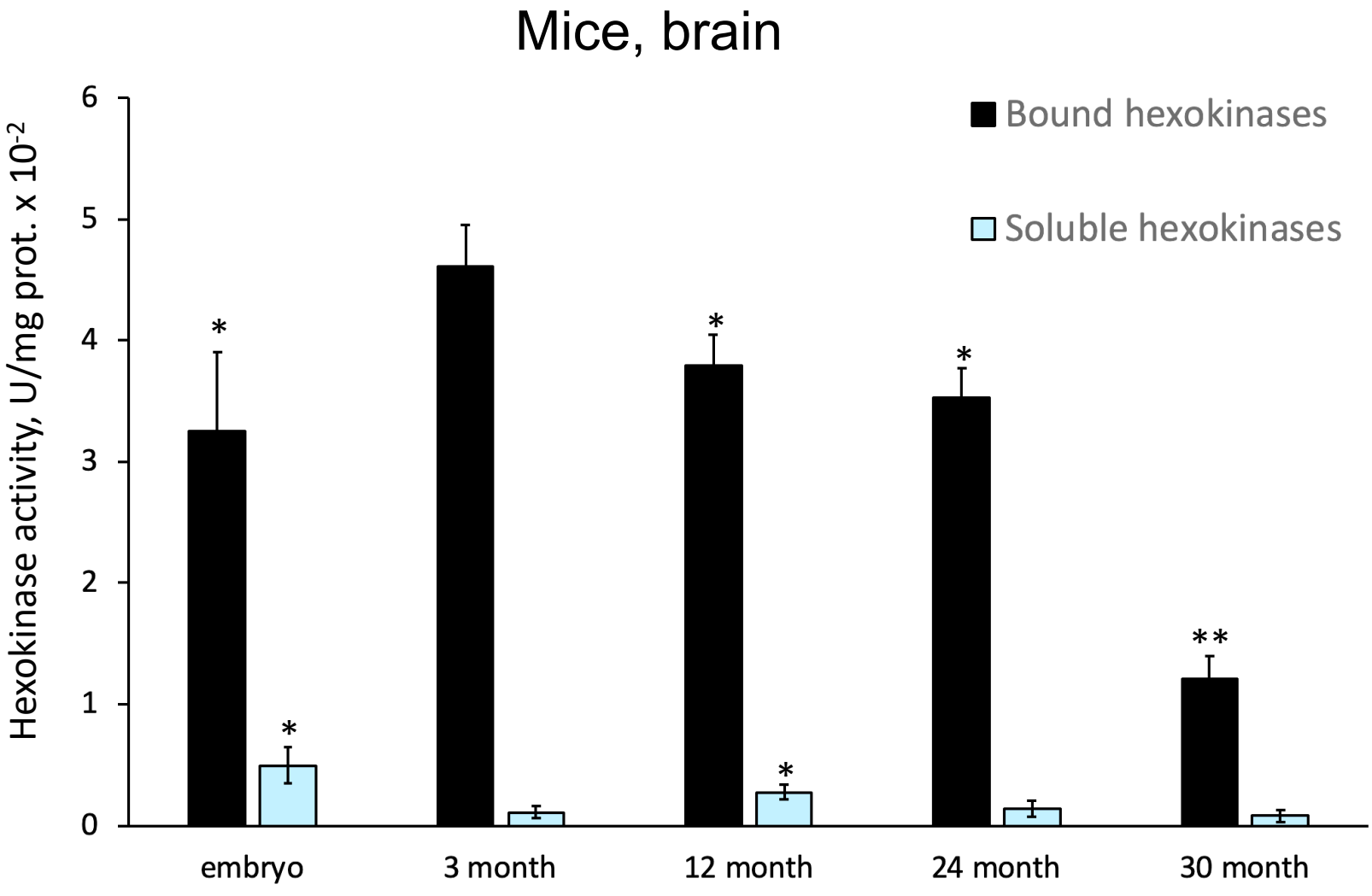

Fig. S14. Hexokinase activity in brain mitochondria and cytosol from mouse embryos and mice of different ages. 3-month-old mice were used for comparison.

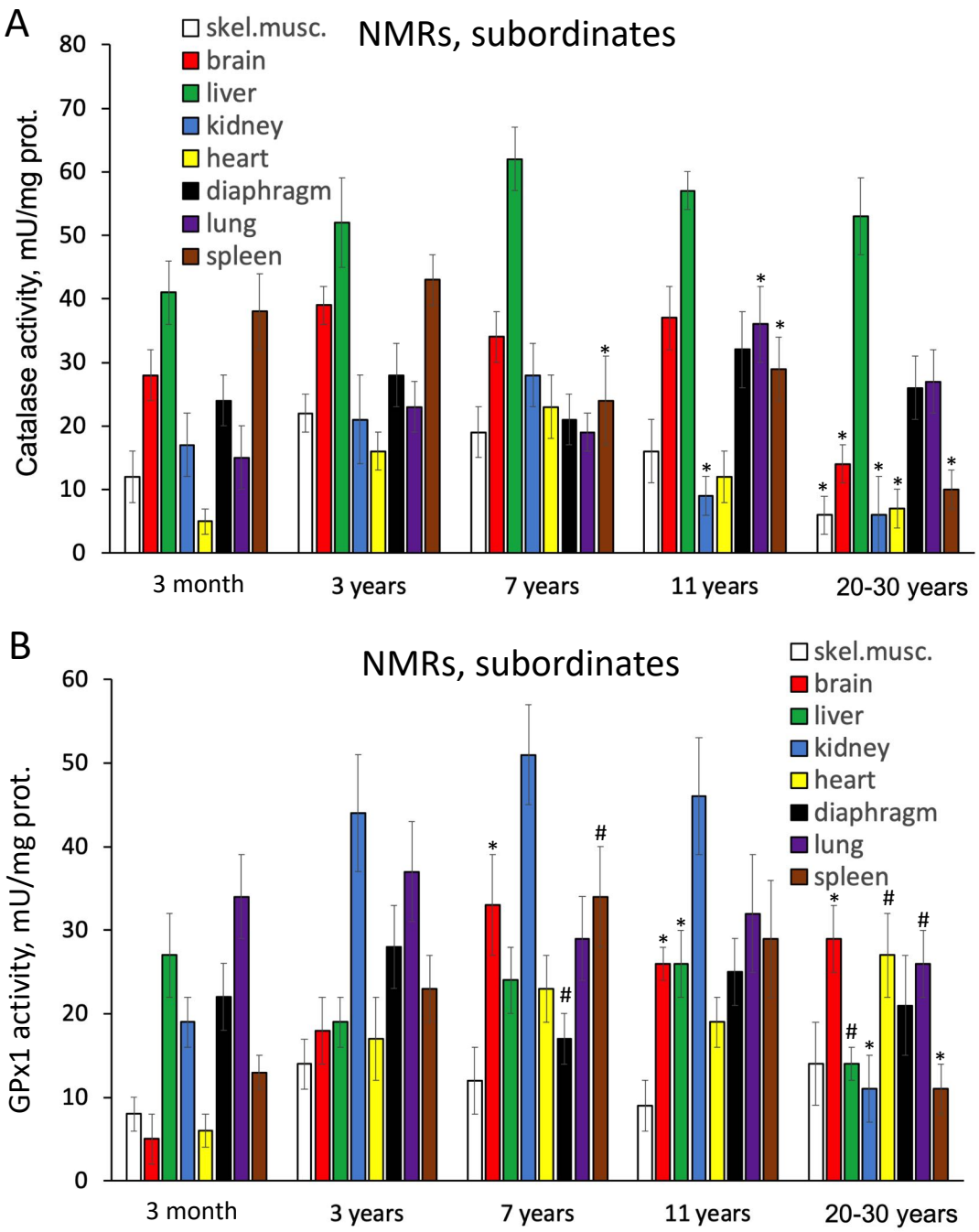

Fig. S15. Activities of catalase (A) and GPx1 (B) in NMR tissues. The effects of aging are shown. 3-month-old NMR subordinates were used for comparison.

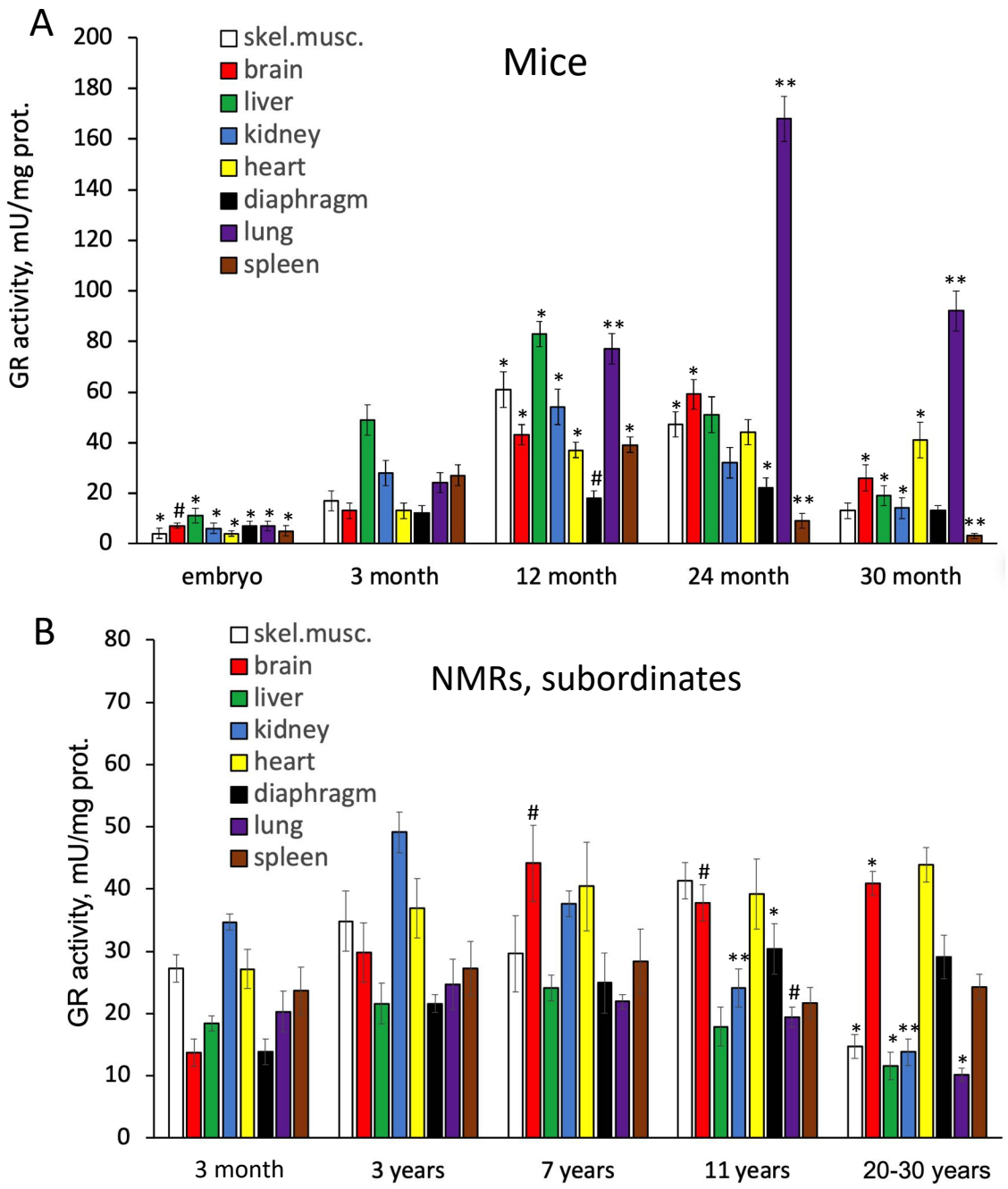

Fig. S16. Activities of glutathione reductase (GR) in mouse (A) and NMR (B) tissues. The effects of aging are shown. 3-month-old animals were used for comparison.

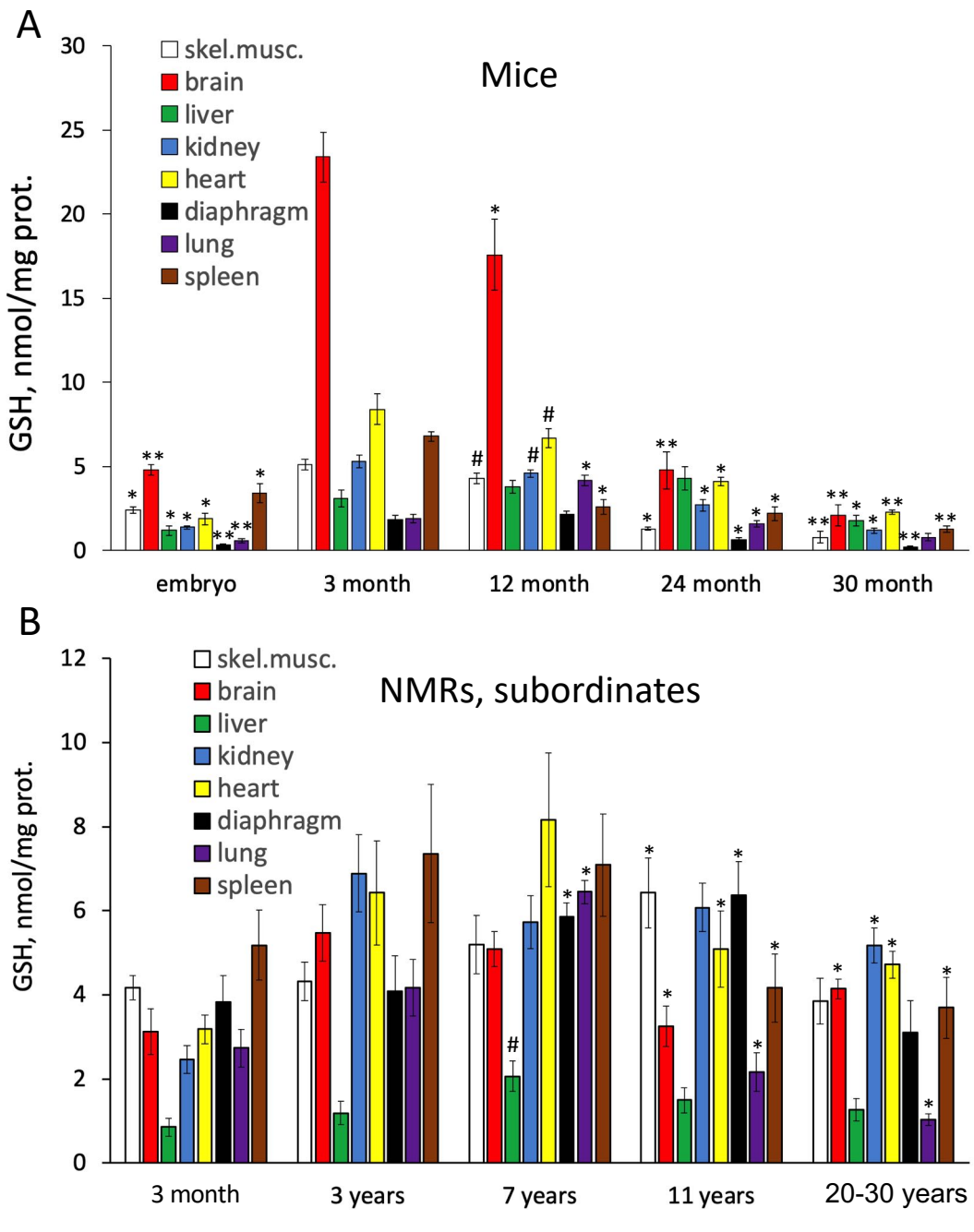

Fig. S17. Amount of reduced glutathione (GSH) in mouse (A) and NMR (B) tissues. The effects of aging are shown. 3-month-old animals were used for comparison.

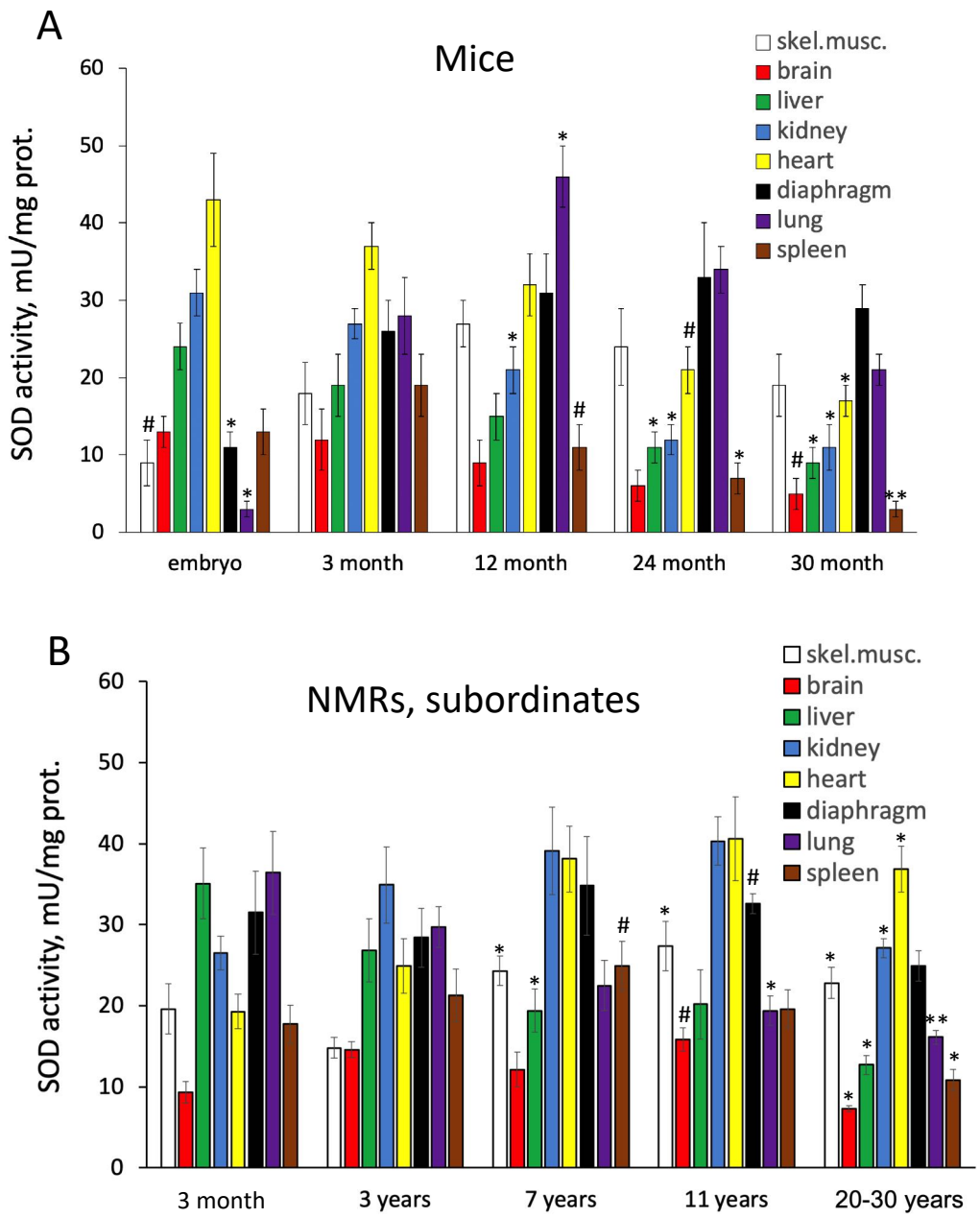

Fig. S18. Superoxide dismutase (SOD) activity in mouse (A) and NMR (B) tissues. The effects of aging are shown. 3-month-old animals were used for comparison.

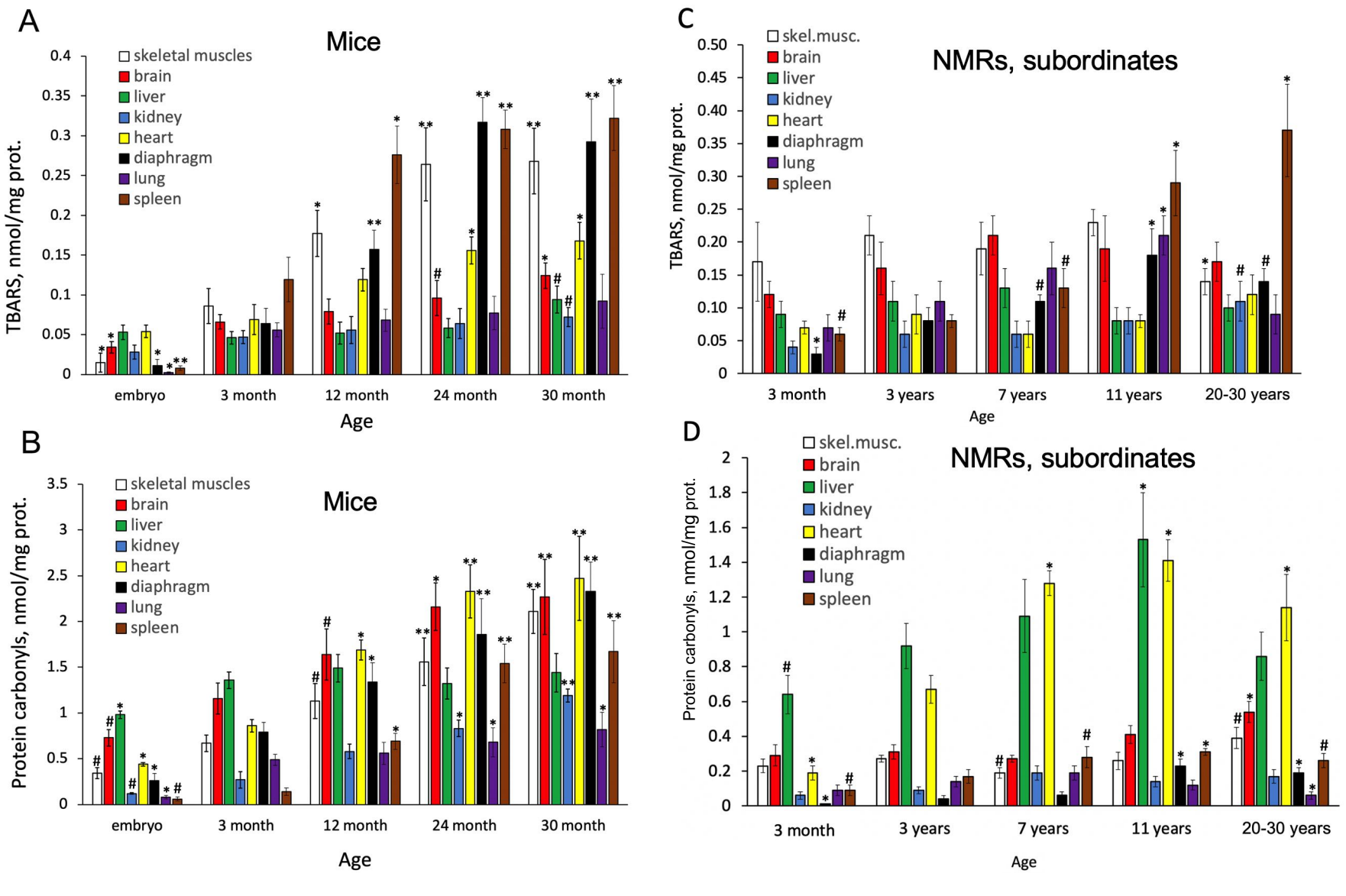

Fig. S19. Malondialdehyde (TBARs probes, A) and protein carbonylation (B) levels in tissues from mice and NMRs of various ages. See Fig. 7 for data from mouse tissues. 3-month-old mice were used for comparison.

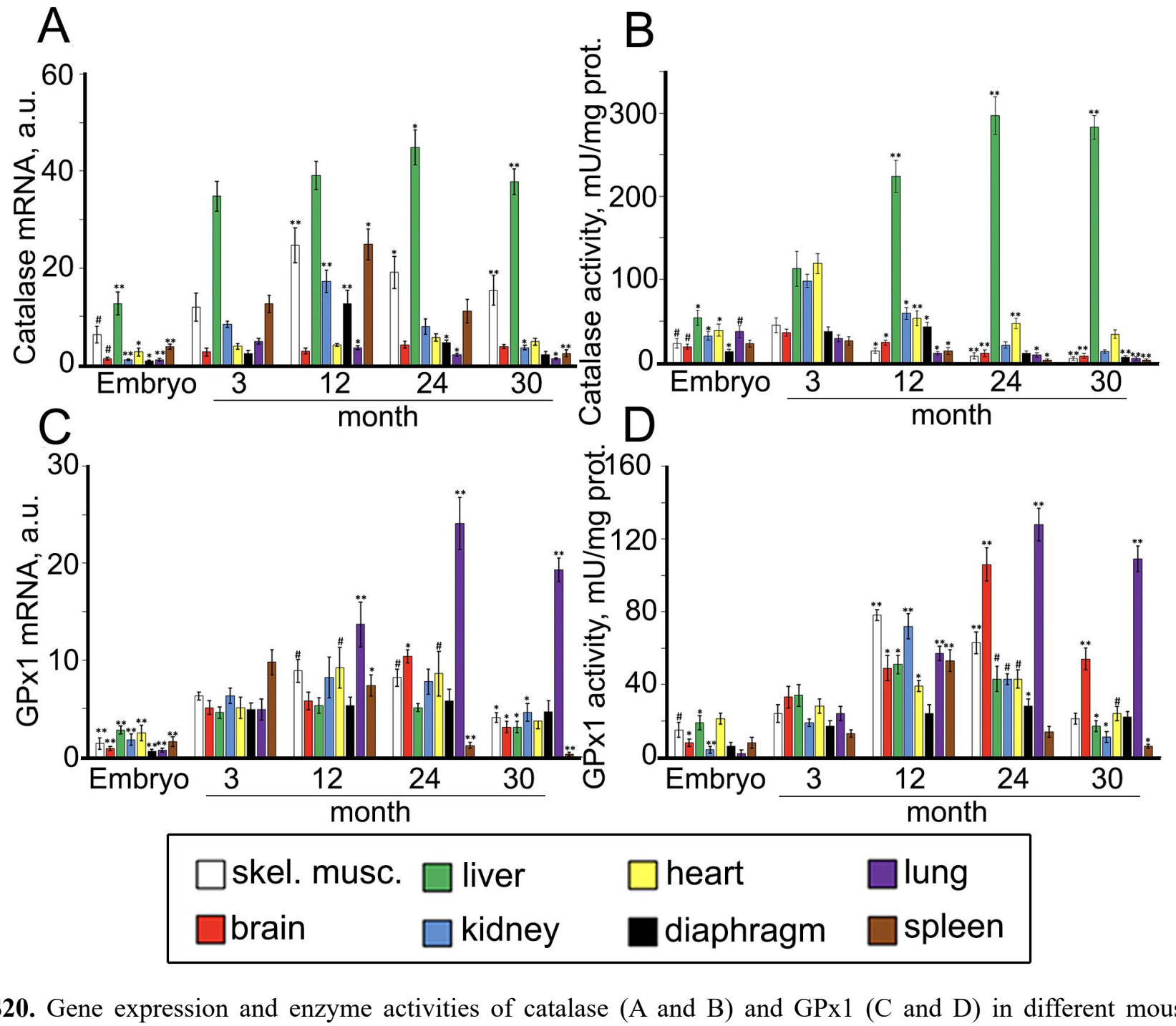

Fig. S20. Gene expression and enzyme activities of catalase (A and B) and GPx1 (C and D) in different mouse tissues; the effect of aging. #, * and **, *p* values are <0.05, 0.01 and 0.001, respectively (mouse embryos and 12-, 24- or 30-month-old mice were compared with 3-month-old mice).

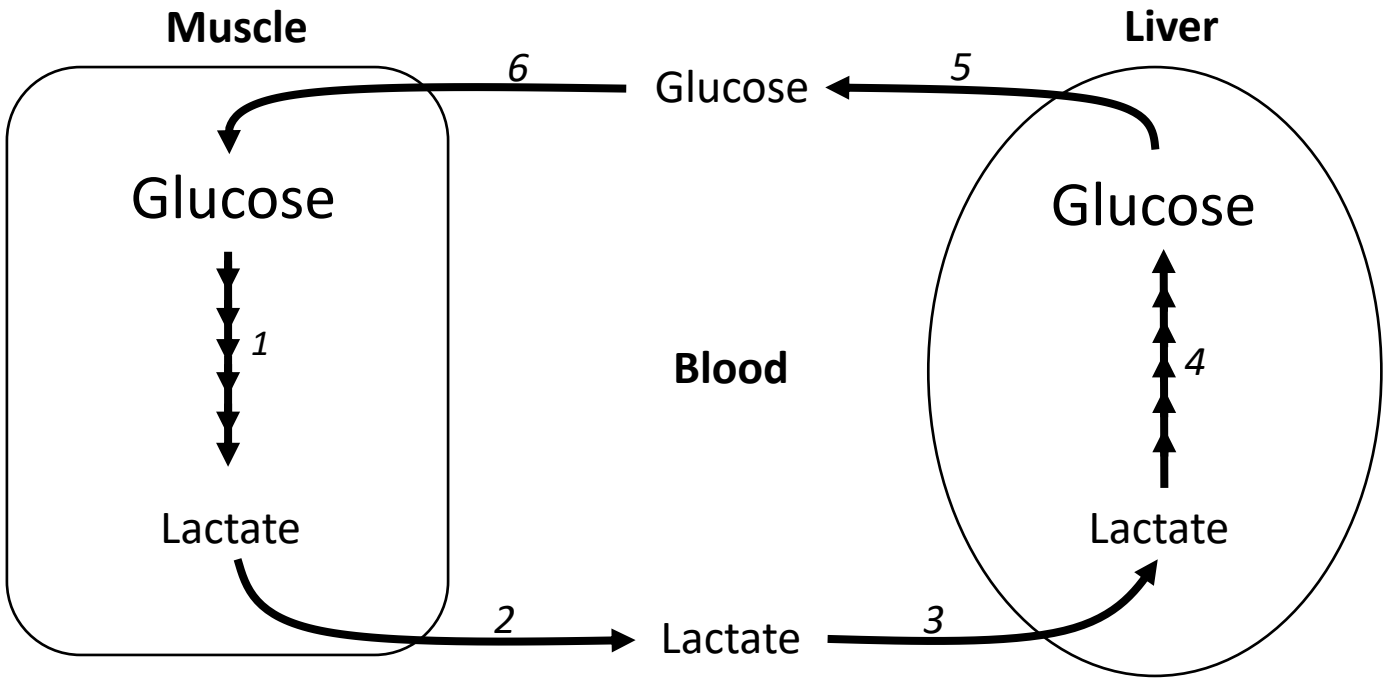

Fig. S21. The Cori cycle. In intensively working skeletal muscles, glucose is converted to lactate by glycolysis. Lactate is transported by the blood to the liver. Here, lactate is converted to glucose or glycogen by reversing the glycolysis reaction (39).

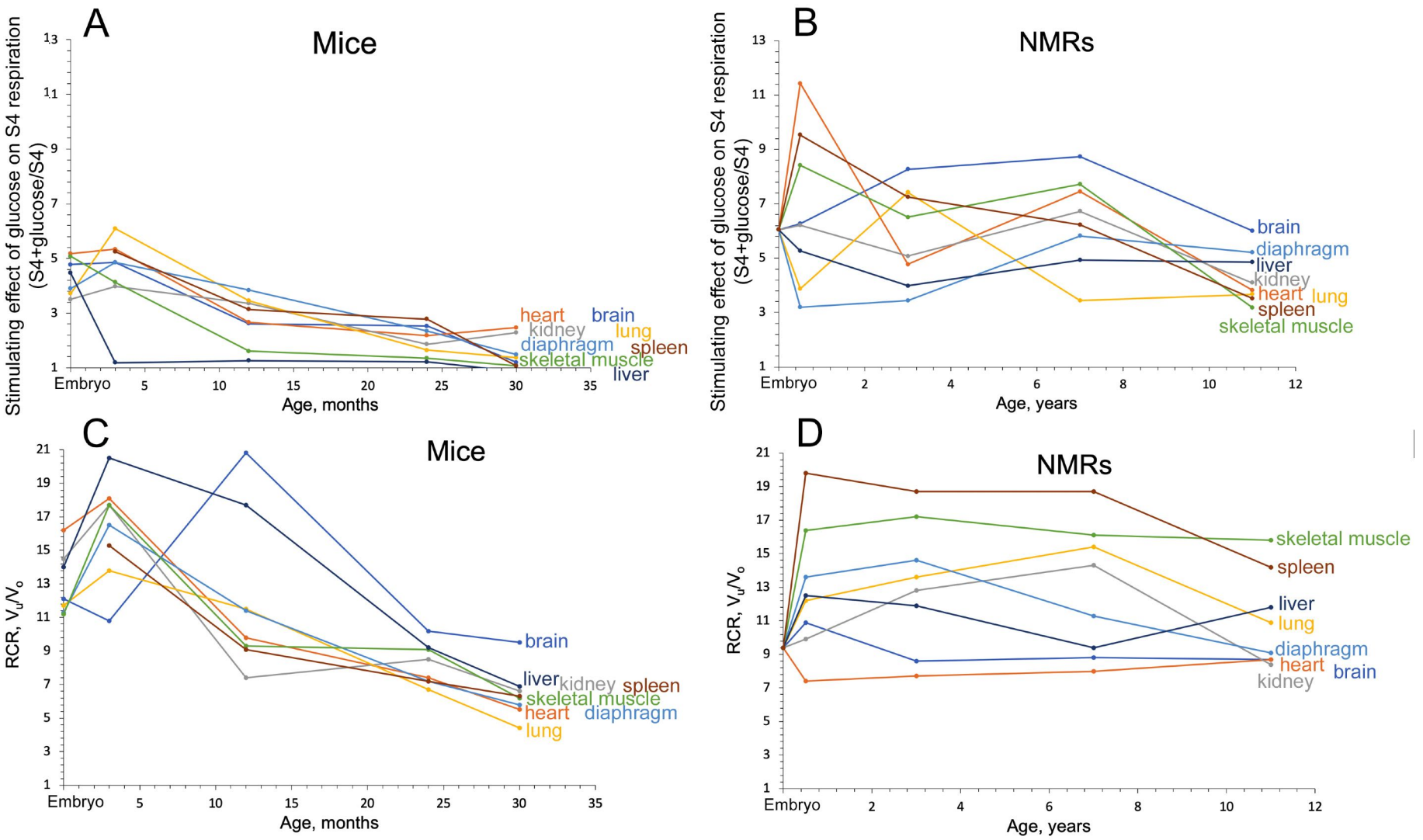

Fig. S22. Stimulation of State 4 respiration by glucose disappears with age in mice (A) but not in NMRs (B). In mice, the respiratory control ratio (RCR) decreased with age, but this decrease was lower than that on glucose stimulation of respiration (C). In NMRs, the RCR does not depend upon age (D). RCR was measured as the ratio of (i) State 3u respiration rate in the presence of the uncoupler FCCP to (ii) State 4o (respiration rate after oligomycin addition).

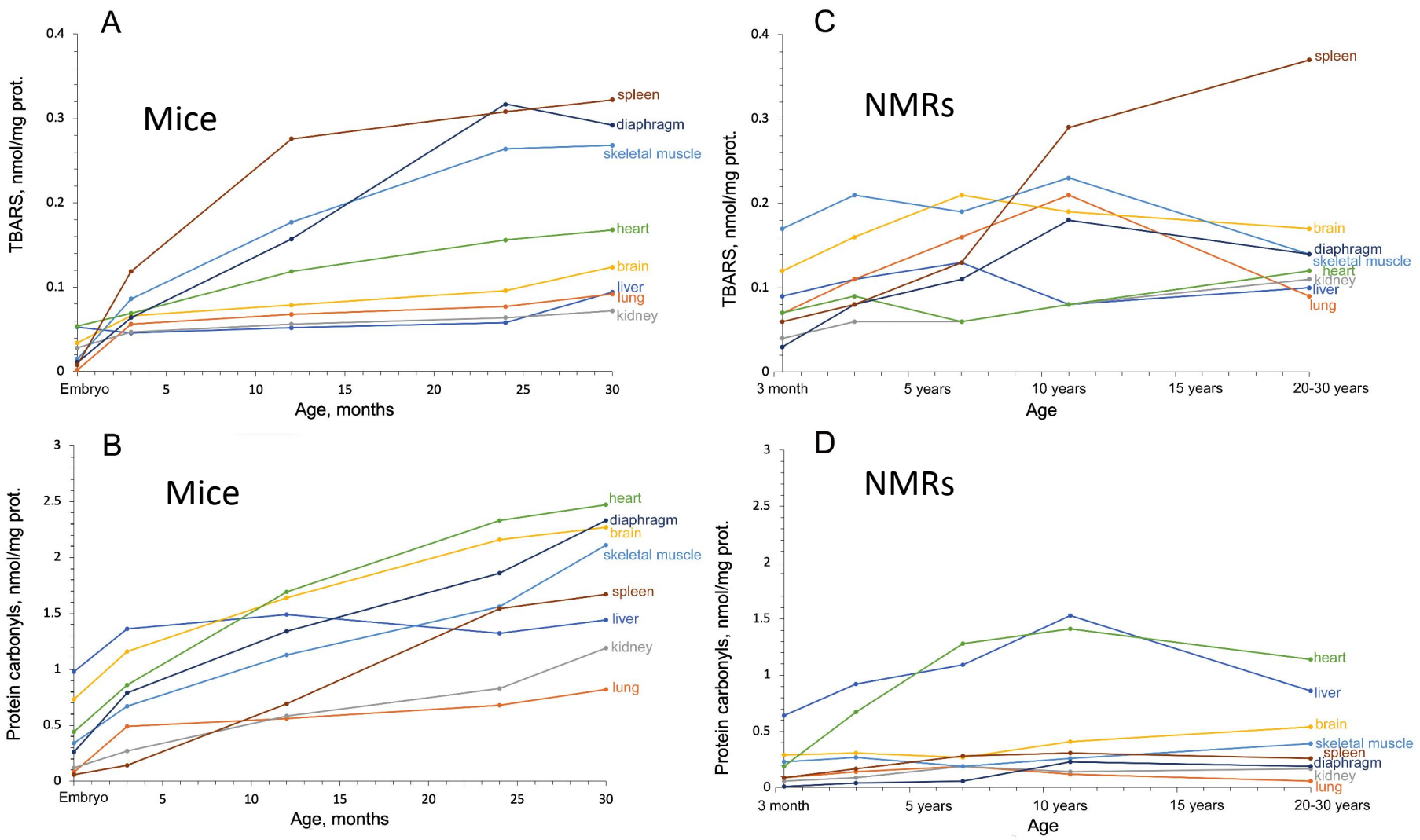

Fig. S23. The disappearance of mild depolarization with age induces oxidative lipid and protein stress in mouse tissues. A, B, The malondialdehyde level (TBARS probe, lipid peroxidation) and protein carbonylation level are shown. C, D, Such effects are absent in the majority of tissues in NMRs who maintain depolarization for many years.

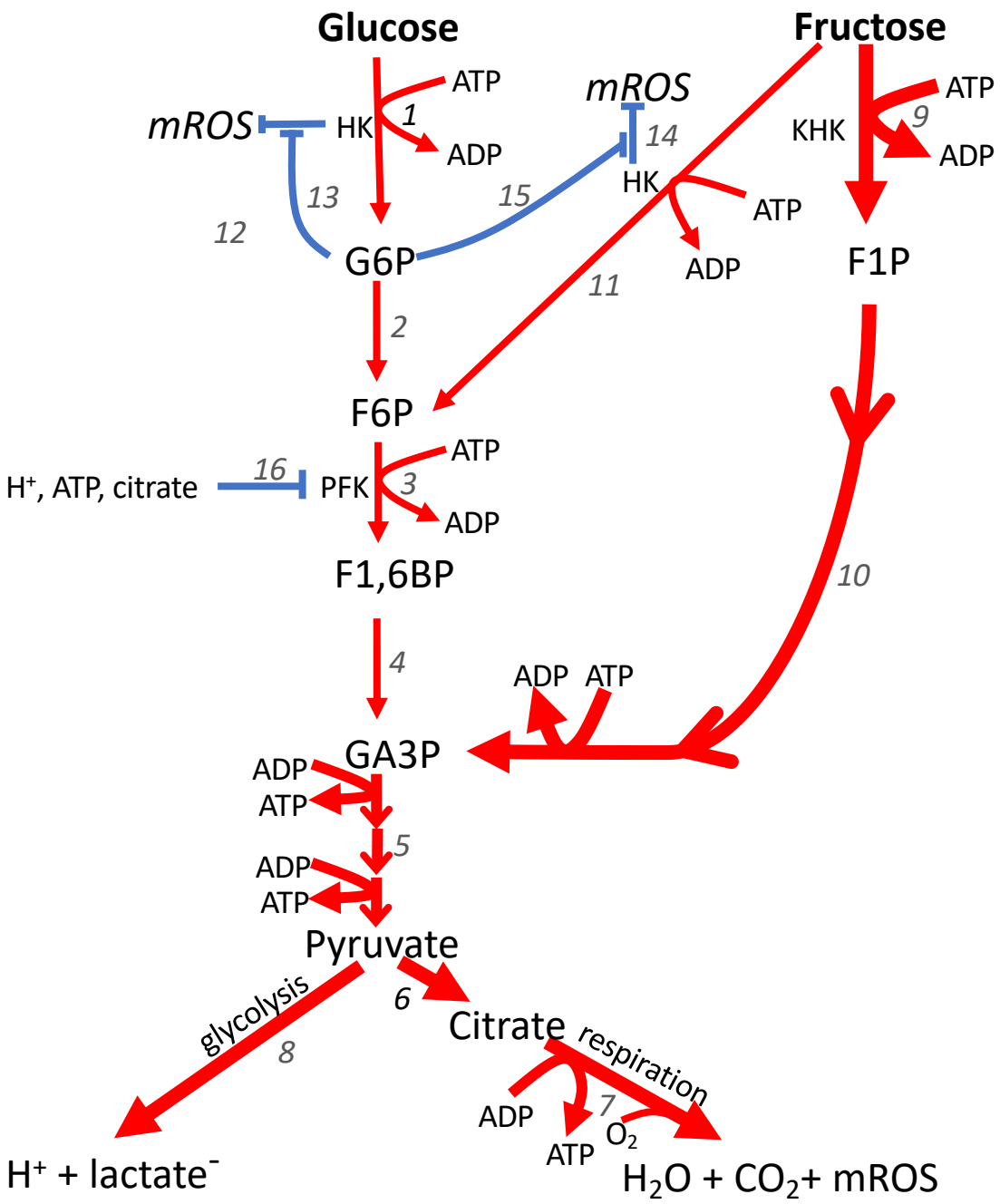

Fig. S24. Glycolysis and fructolysis: chains of events (red) and regulatory steps (blue). 12, The production of mROS is inhibited by mild depolarization mediated by hexokinases I and II (HK). 13, G6P inhibits event 12 by (i) desorbing HK from the mitochondria and (ii) inhibiting the HK catalytic activity. 14, Mild depolarization induced by fructose. 15, Its arrest by G6P. 16, Inhibition of phosphofructokinase (PFK) by products of reactions occurring downstream of PFK [H^+ is formed due to lactic acid deprotonation; ATP is produced by glycolysis and respiration; citrate is formed in the Krebs cycle]. Other abbreviations: F6P, fructose 6-phosphate; F1,6BP, fructose 1,6-bis-phosphate; KHK, ketohexokinase; F1P, fructose 1-phosphate.

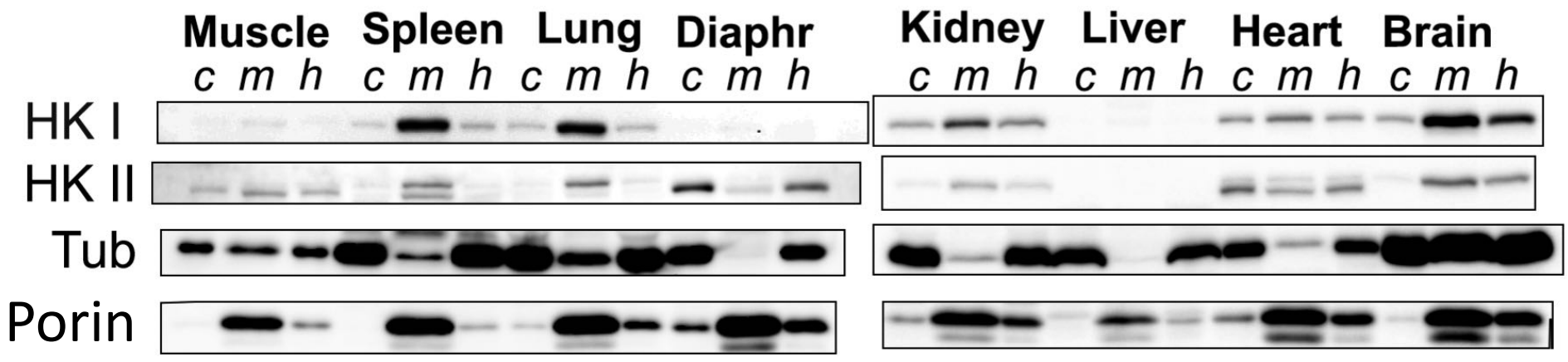

Fig. S25. Representative western blot showing the HK levels in different tissues from a 30-month-old mouse. c, cytosol; m, mitochondria; h, homogenate; Tub, tubulin.

Table S1. Lines of antiROS defense

The type of defense	Prevention of ROS generation	Quenching of already generated ROS
Lowering of [O_2] in the tissues	+	-
Mild depolarization of mitochondria	+	-
Antioxidants (enzymes and small molecules)	-	+

Table S2. Age-related changes in various tissues of 30 month mice vs. 3 month mice

Tissue	Mild depolarization	Amount of bound hexokinases		Activity of antioxidant enzymes		Oxidative stress	
		I	II	Catalase	GPx	Lipid peroxidation	Protein carbonylation
Skeletal muscle	Switch off	Strong decrease	Strong decrease	Decrease	No changes	Increase	Strong increase
Heart	Switch off	Decrease	Decrease	No changes	No changes	Increase	Strong increase
Diaphragm	Switch off	Strong decrease	Decrease	Decrease	No changes	Increase	Strong increase
Spleen	Switch off	Decrease	Strong decrease	Decrease	Decrease	Increase	Strong increase
Brain	Switch off	Decrease	Small at any age	Decrease	No changes	Slight increase	Strong increase
Liver	Switch off	Disappearance	Disappearance	Strong increase	No changes	No changes	No changes
Kidney	Weakening	Decrease	Slight increase	Decrease	No changes	No changes	Strong increase
Lung	Weakening	Decrease	Decrease	Decrease	Strong increase	Slight increase	Slight increase

Table S3. Respiratory parameters of mitochondria from different tissues of mouse (*Mus musculus*), naked mole rat (*Heterocephalus glaber*) and bat (*Carollia perspicillata*).
S2 (succ), State 2 respiration limited by absence of ADP; **succ**, respiratory substrate (10 mM succinate). **State3**, respiration immediately after addition of 100 μM ADP. **State** 4, respiration after exhaustion of added ADP. **S4+gluc**, State 4 respiration after addition of 1 mM glucose. **Oligo**, State 4 respiration after addition of glucose and 10^{-6} M oligomycin. **S3u (FCCP)**, maximal rate of respiration uncoupled by 10^{-7} M FCCP. **RCR (S3u/oligo)**, respiratory control ratio (ratio of respiration rates in State 3u to that in Oligo). **P/O**, ratio of amount of added ADP to consumed O_2 during State 3.

Mouse	Embryo (18-19 days)	3 month	12 month	24 month	30 month
Brain	**n=5**	**n=9**	**n=7**	**n=5**	**n=5**
S2(succ.)	1.4±1.1	2.3±0.9	1.8±1.2	2.6±0.8	3.6±1.9
S3(100μM ADP)	11.9±2.1	18.8±2.4	16.9±1.9	14.9±2.1	18.1±4.6
S4	1.8±0.8	2.7±1.3	3.1±1.2	1.9±0.3	2.6±1.7
S4+gluc.	8.6±1.1	13.1±1.6	8.1±2.3	4.8±1.7	3.1±1.3
Oligo	1.1±0.6	2.2±0.8	1.3±0.4	1.8±0.6	2.1±1.5
S3u (FCCP)	13.4±2.7	23.8±3.9	27.2±3.6	18.4±2.7	19.9±4.7
RCR(S3u/oligo)	12.1±2.8	10.8±2.1	20.8±4.1	10.2±1.7	9.47±3.8
P/O	2.14±0.34	2.49±0.51	2.78±1.11	2.32±0.92	2.08±0.6
Heart	**n=5**	**n=9**	**n=12**	**n=10**	**n=9**
S2(succ.)	2.1±1.3	2.6±0.9	2.8±1.1	3.2±1.4	2.2±0.9
S3(100μM ADP)	13.9±2.7	19.2±2.1	22.4±3.2	16.9±1.8	12.9±2.3
S4	1.8±0.9	2.4±1.3	4.1±1.3	3.8±0.9	3.2±1.4
S4+gluc.	9.3±1.6	12.8±3.2	10.9±1.6	8.3±2.4	7.9±1.6
Oligo	1.2±0.6	1.3±0.7	2.1±0.8	2.4±0.6	2.6±0.7
S3u (FCCP)	19.4±2.8	23.8±4.1	20.7±4.2	17.8±2.8	14.3±1.7
RCR(S3u/oligo)	16.2±2.1	18.1±1.9	9.8±1.6	7.4±1.8	5.5±1.1
P/O	2.5±0.43	2.69±0.74	2.08±0.21	1.76±0.81	1.69±0.23
Kidney	**n=5**	**n=7**	**n=12**	**n=10**	**n=9**
S2(succ.)	1.8±0.4	2.3±1.1	3.1±0.9	2.6±0.7	3.3±1.8
S3(100μM ADP)	12.7±1.6	14.9±2.1	15.3±3.8	16.9±1.7	11.3±1.8
S4	2.8±0.7	3.1±1.9	3.4±1.6	3.6±1.1	2.1±0.6
S4+gluc.	9.8±2.4	12.3±2.2	11.4±1.3	6.7±1.9	4.8±1.7
Oligo	1.1±0.3	1.4±0.8	2.6±0.2	2.4±1.1	2.0±0.4
S3u (FCCP)	15.9±1.7	24.9±5.1	19.3±3.8	20.4±3.7	13.3±1.2
RCR(S3u/oligo)	14.5±1.8	17.7±2.8	7.4±2.1	8.5±1.3	6.6±17
P/O	1.91±0.53	2.17±0.68	2.83±0.74	2.09±0.37	1.71±0.19
Lung	**n=3**	**n=5**	**n=7**	**n=10**	**n=9**
S2(succ.)	2.1±0.2	2.3±0.4	1.5±0.8	2.6±1.1	2.8±0.7
S3(100μM ADP)	10.8±1.6	13.4±1.1	14.8±2.0	12.5±1.9	9.4±1.2
S4	2.4±0.9	2.1±0.6	2.2±0.3	3.1±0.8	2.4±0.5
S4+gluc.	8.9±1.7	12.8±2.2	7.6±1.4	5.1±1.3	3.3±1.8
Oligo	1.2±0.2	1.4±0.6	1.9±0.3	2.4±0.7	2.6±1.1

S3u (FCCP)	14.1±1.8	19.3±2.6	21.9±3.7	16.1±3.2	11.4±2.6
RCR(S3u/oligo)	11.7±2.4	13.8±1.6	11.5±1.9	6.7±2.1	4.4±1.5
P/O	1.92±0.41	2.34±0.57	2.62±0.36	2.44±0.73	2.09±0.24
Diaphragm	**n=3**	**n=5**	**n=7**	**n=10**	**n=9**
S2(succ.)	1.9±0.4	2.1±0.2	2.8±0.7	4.1±1.8	3.1±0.6
S3(100µM ADP)	14.8±1.1	19.7±2.3	16.8±1.7	12.6±2.4	14.3±3.1
S4	2.8±0.7	3.4±1.6	3.2±1.8	2.6±0.7	2.3±0.4
S4+gluc.	10.9±1.3	16.5±2.4	12.3±4.1	6.1±0.8	3.4±1.2
Oligo	1.8±0.3	1.6±0.7	1.9±0.4	2.4±0.5	2.6±0.3
S3u (FCCP)	20.3±1.8	26.4±2.9	21.7±2.2	17.3±2.8	15.1±3.4
RCR(S3u/oligo)	11.3±2.4	16.5±1.3	11.4±1.9	7.2±1.8	5.8±2.4
P/O	2.29±0.47	2.43±0.39	2.78±0.52	2.31±0.47	2.19±0.83
Skeletal muscle	**n=5**	**n=7**	**n=12**	**n=10**	**n=9**
S2(succ.)	2.6±0.7	3.4±1.1	2.3±0.4	2.9±0.6	2.1±0.9
S3(100µM ADP)	15.8±2.1	19.3±2.4	23.1±1.9	14.2±1.7	12.7±2.2
S4	2.8±0.2	3.9±1.6	4.3±1.5	3.2±0.7	4.1±1.8
S4+gluc.	14.2±2.7	16.1±1.4	6.9±1.3	4.3±0.8	4.4±1.1
Oligo	1.9±0.3	1.6±0.8	2.4±0.5	1.9±0.2	2.4±0.4
S3u (FCCP)	21.3±2.8	28.4±1.6	22.3±2.4	17.3±3.8	14.8±1.9
RCR(S3u/oligo)	11.2±2.4	17.7±2.7	9.3±1.8	9.1±2.6	6.2±1.3
P/O	1.83±0.24	1.96±0.34	2.36±0.51	2.09±0.48	2.33±0.61
liver	**n=5**	**n=7**	**n=12**	**n=10**	**n=9**
S2(succ.)	2.6±0.8	3.4±1.5	3.6±1.3	4.4±2.1	4.6±1.3
S3(100µM ADP)	16.9±2.1	24.3±1.8	21.7±3.4	19.3±1.1	17.9±3.8
S4	3.2±0.9	5.4±2.3	4.2±1.8	5.1±1.7	6.3±1.4
S4+gluc.	14.3±2.6	6.4±1.3	5.3±1.8	6.2±0.9	5.4±1.6
Oligo	2.1±0.7	1.6±0.2	1.6±0.4	2.4±0.7	2.6±0.5
S3u (FCCP)	29.4±5.1	32.3±4.8	28.4±6.2	22.1±1.9	18.1±2.3
RCR(S3u/oligo)	14.0±2.8	20.2±5,3	17.7±4.1	9.2±3.4	6.9±1.7
P/O	1.61±0.39	1.89±0.47	1.77±0.64	2.11±0.36	2.29±0.27
spleen	**nd**	**n=7**	**n=12**	**n=10**	**n=9**
S2(succ.)		2.1±0.3	2.4±0.8	1.3±0.7	2.6±0.3
S3(100µM ADP)		19.4±2.7	16.4±1.3	15.1±2.3	17.8±2.1
S4		3.2±1.4	3.6±1.1	2.3±0.9	4.2±1.6
S4+gluc.		16.8±2.1	11.3±2.4	6.4±2.1	4.5±0.7
Oligo		1.8±0.2	2.1±0.4	2.4±0.7	2.9±1.3
S3u (FCCP)		28.1±4.2	19.2±1.3	17.3±2.8	18.4±4.1
RCR(S3u/oligo)		15.3±1.1	9.1±2.4	7.2±1.3	6.3±1.8
P/O		2.57±0.34	2.73±0.19	2.14±0.61	1.59±0.22
NMR	**Embryo (20-30 days)**	**0.5 year**	**3 years**	**7 years**	**11 years**
Brain	**n=3**	**n=7**	**n=5**	**n=5**	**n=3**
S2(succ.)	3.6±1.9	4.2±1.8	3.1±0.7	3.4±1.2	4.2±1.3

S3(100µM ADP)	19.6±3.1	28.3±3.5	24.8±3.3	27.4±3.8	26.2±4.9
S4	2.3±0.2	2.7±1.3	2.2±0.6	2.6±0.8	3.3±1.4
S4+gluc.	13.9±2.2	16.9±4.1	18.2±4.1	22.7±3.8	19.8±2.7
Oligo	2.9±1.1	3.2±1.1	4.4±1.5	3.6±0.9	3.9±1.7
S3u (FCCP)	27.4±4.7	34.9±6.2	37.9±5.2	31.7±4.5	33.9±7.3
RCR(S3u/oligo)	9.4±1.6	10.9±3.4	8.6±2.2	8.8±1.6	8.7±2
P/O	1.73±0.28	2.02±0.34	2.14±0.23	1.89±0.31	2.19±0.28
Heart	**n=3**	**n=7**	**n=5**	**n=5**	**n=3**
S2(succ.)	3.6±1.9	1.9±0.3	2.5±0.8	2.9±0.6	3.7±1.4
S3(100µM ADP)	19.6±3.1	22.4±1.9	20.9±2.3	23.8±3.7	18.7±4.1
S4	2.3±0.2	1.6±0.5	3.6±1.7	2.9±1.2	3.9±1.7
S4+gluc.	13.9±2.2	18.3±4.1	17.2±2.4	21.6±4.8	14.9±2.2
Oligo	2.9±1.1	3.3±1.2	3.6±1.3	3.1±1.2	2.9±0.3
S3u (FCCP)	27.4±4.7	24.6±2.1	27.8±3.2	24.9±5.1	25.2±4.8
RCR(S3u/oligo)	9.4±1.6	7.4±1.3	7.7±1.9	8±1.6	8.7±1.6
P/O	1.73±0.28	2.35±0.19	2.11±0.36	2.73±0.61	2.26±0.49
Kidney	**n=3**	**n=7**	**n=5**	**n=5**	**n=3**
S2(succ.)	3.6±1.9	3.8±0.6	2.6±0.4	2.1±0.8	3.8±1.4
S3(100µM ADP)	19.6±3.1	21.9±4.7	23.7±4.2	24.3±3.6	19.3±2.7
S4	2.3±0.2	2.8±1.6	3.9±1.7	2.5±0.7	3.4±1.2
S4+gluc.	13.9±2.2	17.4±3.1	19.8±2.4	16.8±2.1	13.9±2.3
Oligo	2.9±1.1	3.1±0.8	3.4±1.3	1.9±0.4	3.8±0.7
S3u (FCCP)	27.4±4.7	30.6±2.8	33.9±6.1	27.1±2,3	32.1±4.8
RCR(S3u/oligo)	9.4±1.6	9.9±1.7	10±2,3	14.3±2.8	8.4±1.6
P/O	1.73±0.28	2.29±0.36	2.08±0.17	2.41±0.13	1.99±0.26
Lung	**n=3**	**n=7**	**n=5**	**n=5**	**n=3**
S2(succ.)	3.6±1.9	4.8±2.1	4.1±1.1	3.9±0.4	4.4±2.1
S3(100µM ADP)	19.6±3.1	17.1±4.5	20.9±5.7	22.8±4.5	18.9±3.6
S4	2.3±0.2	3.8±1.2	2.4±0.7	4.1±1.3	3.7±0.8
S4+gluc.	13.9±2.2	14.7±3.8	17.8±3.1	14.1±3.8	13.6±2.4
Oligo	2.9±1.1	1.9±0.7	2.5±0.9	2.1±0.6	2.8±0.9
S3u (FCCP)	27.4±4.7	23.2±4.6	34.1±5.8	32,3±6.4	30.5±4.9
RCR(S3u/oligo)	9.4±1.6	12.2±3.8	13.6±2.1	15.4±3.7	10.9±2.4
P/O	1.73±0.28	2.46±0.38	1.87±0.28	2.29±0.33	1.86±0.49
Diaphragm	**n=3**	**n=7**	**n=5**	**n=5**	**n=3**
S2(succ.)	3.6±1.9	2.6±0.8	2.1±0.3	3.9±0.7	2.9±0.3
S3(100µM ADP)	19.6±3.1	17.3±3.4	20.4±3.1	24.3±1.9	21.8±3.1
S4	2.3±0.2	4.2±1.8	4.6±2.2	3.4±1.3	3.9±1.4
S4+gluc.	13.9±2.2	13.4±1.7	15.8±2.4	19.8±4.1	20.3±2.
Oligo	2.9±1.1	1.9±0.8	2.3±0.9	3.2±0.8	3.1±0.7

S3u (FCCP)	27.4±4.7	21.5±4.9	34.3±4.8	36.1±5.8	28.3±4.9
RCR(S3u/oligo)	9.4±1.6	13.6±3.1	14.6±3.1	11.3±2.9	9,1±1.8
P/O	1.73±0.28	1.84±0.42	2,49±0.51	2.63±0.27	1.91±0.14
Skeletal muscle	**n=3**	**n=7**	**n=5**	**n=5**	**n=3**
S2(succ.)	3.6±1.9	4.5±1.7	3.7±0.8	4.1±1.2	4.8±1.7
S3(100µM ADP)	19.6±3.1	17.8±3.1	27.2±4.8	23.8±3.6	19,4±3.2
S4	2.3±0.2	1.7±0.9	3,5±1.4	2.5±0.8	3.8±1.6
S4+gluc.	13.9±2.2	14.3±2.6	22.8±3.6	19.3±2.1	12.1±2.8
Oligo	2.9±1.1	1.3±0.4	1.9±0.8	1.6±0.5	1.8±0.5
S3u (FCCP)	27.4±4.7	21.1±3.9	24.9±3.7	25.6±4.7	16.8±2.4
RCR(S3u/oligo)	9.4±1.6	16.4±3.2	13.1±2.4	16,1±3.8	15.8±3.1
P/O	1.73±0.28	2.11±0.13	2.54±0.47	1.93±0.36	2.78±0.66
liver	**n=3**	**n=7**	**n=5**	**n=5**	**n=3**
S2(succ.)	3.6±1.9	2.8±0.4	3.1±0.4	3.9±1.1	3.4±0.8
S3(100µM ADP)	19.6±3.1	22.7±3.1	24.9±4.2	21.8±1.9	19.3±4.1
S4	2.3±0.2	3.8±1.5	4.8±2.3	3.2±0.6	2.8±1.1
S4+gluc.	13.9±2.2	20±4.8	19.1±3.4	15.8±3.2	13.6±2.4
Oligo	2.9±1.1	2.2±0.6	2.8±0.7	3.3±1.4	2.1±0.7
S3u (FCCP)	27.4±4.7	27.5±2,1	25.3±1.9	30.9±4.7	24.8±4.6
RCR(S3u/oligo)	9.4±1.6	12.5±2.7	9.2±1.9	9.4±2.2	11.8±1.3
P/O	1.73±0.28	2,14±0.28	2,29±0.31	1.69±0.19	2.54±0.41
spleen	**n=3**	**n=7**	**n=5**	**n=5**	**n=3**
S2(succ.)	3.6±1.9	1.6±0.4	2.1±03	3.4±1.9	2.9±0.7
S3(100µM ADP)	19.6±3.1	18.2±3.1	24.2±3.8	26.4±4.5	22.8±3.6
S4	2.3±0.2	1.3±0.7	2.4±0.9	3.5±1.1	4.8±1.3
S4+gluc.	13.9±2.2	12.4±3.1	17.4±3.1	21.8±3.1	16.9±4.2
Oligo	2.9±1.1	1.1±0.3	2.4±1.3	1.8±0.3	2.2±0.8
S3u (FCCP)	27.4±4.7	21.8±3.6	28.9±4.7	34.2±3.9	31.3±2.9
RCR(S3u/oligo)	9.4±1.6	19.8±4.2	12±3.8	18.7±2.9	14.2±2.6
P/O	1.73±0.28	2.83±0.64	2.02±0.27	1.89±0.25	2.19±0.36

Car. persp.	**Very young**	**Young**	**Adult**	**Old**
Heart	**n=3**	**n=3**	**n=3**	**n=3**
S2(succ.)	2,7±0,4	1.96±0.31	1.32±0.18	2.09±0.83
S3(100µM ADP)	19.4±4,1	31.92±4.8	29.14±3.27	22.14±3.8
S4	3.2±0.8	3.02±0.74	2.97±1.04	4.56±2.11
S4+gluc.	8.8±1.7	5.19±1.2	13.44±3.22	8.37±1.17
Oligo	4.6±1.4	0.76±0.21	1.14±0.27	0.96±0.24
S3u (FCCP)	24.8±3.5	8.8±1.9	23.8±4.5	19.33±4.81
RCR(S3u/oligo)	5.5±1.4	11.62±2.4	20.9±3.8	20.13±3.18
P/O	1.58±0.25	1.94±0.13	2.26±0.37	2.49±0.51

Skeletal muscle	**n=3**	**n=3**	**n=3**	**n=3**
S2(succ.)	1.65±0.38	2.19±0.33	2.47±1.08	1.84±0.33
S3(100µM ADP)	33.17±5.47	36.21±5.09	32.14±6.33	24.08±3.13
S4	3.59±1.14	4.31±2.14	3.28±0.67	5.49±1.97
S4+gluc.	22.17±4.81	19.43±3.47	16.22±4.01	12.28±3.04
Oligo	2.38±0.46	2.68±0.44	2.14±0.49	2.67±0.49
S3u (FCCP)	36.19±6.29	34.12±4.27	30.17±2.51	25.17±3.92
RCR(S3u/oligo)	15.32±3.61	12.73±2.24	14.09±2.96	9.4±1.92
P/O	2.09±0.14	2.33±0.19	2.59±0.61	2.61±0.39